SYNTHESIS AND CHARACTERIZATION OF NANOCRYSTALLINE ZnS:Mn^{2+}_POLYELECTROLYTE

ON-UMA NIMITTRAKOOLCHAI

A THESIS SUBMITTED IN PARTIAL FULFILLMENT
OF THE REQUIREMENTS FOR
THE DEGREE OF MASTER OF SCIENCE
(POLYMER SCIENCE AND TECHNOLOGY)
FACULTY OF GRADUATE STUDIES
MAHIDOL UNIVERSITY
2005

ISBN 974-04-5807-6

Thesis
Entitled

SYNTHSIS AND CHARACTERIZATION OF NANOCRYSTALLINE ZnS:Mn^{2+}-POLYELECTROLYTE

On-uma Nimittvakoolchai
.....
Miss On-uma Nimittrakoolchai
Candidate

Darapond T.
.....
Ms. Darapond Triampo,
Ph.D.
Major-Advisor

.....
Asst.Prof. Toemsak Srikhirin,
Ph.D.
Co-Advisor

Tanakorn Osotchan
.....
Asst.Prof. Tanakorn Osotchan,
Ph.D.
Co-Advisor

Pranee Phinyocheep
.....
Assoc.Prof. Pranee Phinyocheep,
Doctorat de l' Universite' du Maine
Co-Advisor

Rassmidara Hoonsawat
.....
Assoc.Prof. Rassmidara Hoonsawat,
Ph.D.
Dean
Faculty of Graduate Studies

T. Amornsakchai
.....
Assoc.Prof. Taweechai Amornsakchai,
Ph.D.
Chair
Master of Sciece Programme
in Polymer Science and Technology
Faculty of Science

Thesis
Entitled

SYNTHSIS AND CHARACTERIZATION OF NANOCRYSTALLINE ZnS:Mn^{2+}_POLYELECTROLYTE

was submitted to the Faculty of Graduate Studies, Mahidol University
for the degree of Master of Science (Polymer Science and Technology)
on
16 March, 2005

On-uma Nimittrakoolchai
.....
Miss On-uma Nimittrakoolchai
Candidate

Darapond T.
.....
Ms. Darapond Triampo, Ph.D.
Chair

Wannapong Triampo
.....
Asst. Prof. Wannapong Triampo,
Ph.D.
Member

.....
Asst.Prof. Toemsak Srikhirin,
Ph.D.
Member

Tanakorn Osotchan
.....
Asst.Prof. Tanakorn Osotchan,
Ph.D.
Member

Pranee Phinyocheep
.....
Assoc.Prof. Pranee Phinyocheep,
Doctorat de l' Universite' du Maine
Member

Rassmidara Hoonsawat
.....
Assoc.Prof. Rassmidara Hoonsawat,
Ph.D.
Dean
Faculty of Graduate Studies
Mahidol University

Amaret Bhumiratana
.....
Prof. Amaret Bhumiratana,
Ph.D.
Dean
Faculty of Science
Mahidol University

ACKNOWLEDGEMENT

I would like to thank my major advisor, Dr.Darapond Triampo for her excellent comments and very helpful suggestions and kindness. I wish to express my sincere gratitude and deep appreciation to Dr.Toemsak Srikhirin my co-advisor for his guidance, invaluable advice, supervision and encouragement throughout. I am equally grateful to Dr.Tanakorn Osotchan and Dr.Pranee Phinyocheep, my co-advisors for their useful comments, supervision and encouragement. I am also grateful to Dr. Wannapong Triampo, the external examiner for his advice and constructive criticism.

I would like to thank Capability building unit for Nanoscience and Nanotechnology for supporting chemical reagents and instruments in my thesis work.

I would like to thank Dr.Yongyut Kajornpredanon, Dr.Yot Boonthongkong and Mr.Wisithpong Yodsri for using Transmission Electron Microscope. I also would like to thank Mr.Supreecha Charunesak, MDI for using centrifuge machine.

I am particularly indebted to the Faculty of Science, Mahidol University, Thailand for the teaching assistant scholarship which enabled me to undertake this study.

Furthermore, I wish to thank all my teachers, my good friends at Polymer science and technology program for their kindness and helps in various ways. I also would like to thank people at Capability building unit for Nanoscience and Nanotechnology, Sukanya, Thitima, Sirasa, Somporn, Saijai, Sripajak, Anurak and others whose names are not mentioned here for helpful, wonderful friendships. Especially, I would like to thank Kritsanu for his helpful and encouragement.

Finally, a special word of thank is given to my father, mother, sister and brothers for their support, understanding, infinite love and encouragement.

On-uma Nimittrakoolchai

SYNTHESIS AND CHARACTERIZATION OF NANOCRYSTALLINE ZnS:Mn^{2+}_POLYELECTROLYTE.

ON-UMA NIMITRAKOOLCHAI 4537360 SCPO/M

M.Sc. (POLYMER SCIENCE AND TECHNOLOGY)

THESIS ADVISORS: DARAPOND TRIAMPO, Ph.D. (MATERIALS), TOEMSAK SRIKHIRIN, Ph.D. (POLYMER SCIENCE), PRANEE PHINYOCHEEP, DOCTORAL DE L′ UNIVERSITE′ DU MAINE (POLYMER CHEMISTRY), TANAKORN OSOTCHAN, Ph.D. (PHYSICS)

ABSTRACT

This research focuses on the synthesis of inorganic based light emitting materials which have nanometer size and good luminescence properties. A synthesis of Mn-doped ZnS (ZnS:Mn^{2+}) nanocrystalline material was carried out by a liquid phase co-precipitation method. Poly(4-strylenesulfonic acid-co-maleic acid) (PSSA-MA) was used as a surface passivating agent which was fed directly into the reaction medium to control a crystallization process and prevent surface oxidation of materials. A condition of the experiment was adjusted so that a growth of ZnS:Mn^{2+} was limited to a nanocrystallized size. The crystal structure, crystal size and its luminescence properties were investigated and compared to those of unpassivated or bulk samples.

X-ray diffraction (XRD), transmission electron microscope (TEM) and selected area electron diffraction (SAED) show the ZnS:Mn^{2+} nanocrystals to be cubic structure. The calculated crystal size is about 2-3 nm which the passivated sample illustrates a smaller size than unpassivated. The crystallinity of the material was also evident from high resolution transmission electron microscope (HRTEM) which gave well-defined images of crystals with clear lattice fringes. A UV-Vis optical spectroscopy study showed a blue-shift with respect to the bulk value. The photoluminescence (PL) intensity of all samples shows an orange emission peak at 600 nm which characterize for the $^4T_1 \rightarrow {}^6A_1$ transition of Mn^{2+} ion in a crystalline ZnS-matrix. In addition, the passivated sample also shows peak of PSSA-MA at 500 nm, no found in unpassivated. The PL intensity of the passivated sample is higher than that of the unpassivated sample, because the surface passivating agent decreases surface defect and depresses radiationless transitions. The highest PL intensity was obtained when using PSSA-MA 4% w/v. The presence of PSSA-MA that coordinated with nanocrystal sample was confirmed by Fourier transform infrared spectroscopy (FTIR) and thermal gravimetric analysis (TGA).

KEY WORDS : MANGANESE-DOPED ZINC SULFIDE/ NANOCRYSTAL/ PHOTOLUMINESCENCE

73 pp. ISBN 974-04-5807-6

การเตรียมและศึกษาสมบัติของผลึกขนาดนาโนเมตรของผลึกซิงค์ซัลไฟด์ที่ถูกเจือด้วยแมงกานีสไอออนในสภาวะที่มีพอลิอิเลคโทรไลท์ (SYNTHESIS AND CHARACTERIZATION OF NANOCRYSTALLINE ZnS:Mn^{2+}_POLYELECTROLYTE)

อรอุมา นิมิตรตระกูลชัย 4537360 SCPO/M

วท.ม. (วิทยาศาสตร์และเทคโนโลยีพอลิเมอร์)

คณะกรรมการควบคุมวิทยานิพนธ์ : ดาราภรณ์ เตรียมโพธิ์, Ph.D. (MATERIALS), เติมศักดิ์ ศรีคิรินทร์, Ph.D. (POLYMER SCIENCE), ปราณี ภิญโญชีพ, DOCTORAL DE L′ UNIVERSITE′ DU MAINE (POLYMER CHEMISTRY), ธนากร โอสถจันทร์, Ph.D.(PHYSICS)

บทคัดย่อ

งานวิจัยนี้เป็นการศึกษาการสังเคราะห์ซิงค์ซัลไฟด์ที่เจือด้วยแมงกานีสไอออน ซึ่งมีคุณสมบัติเป็นสารเรืองแสงให้มีผลึกขนาดนาโนเมตรและมีคุณสมบัติในการเปล่งแสงที่ดี สารเรืองแสงขนาดนาโนถูกเตรียมโดยวิธีการตกตะกอนในน้ำภายใต้การควบคุมปริมาณของสารพอลิสไตลีนซัลโฟนิกแอสิดโคมาเลอิกแอสิด ซึ่งเป็นสารพอลิอิเลคโทรไลท์ โดยที่ผิวของอนุภาคซิงค์ซัลไฟด์จะดูดซับสารพอลิอิเลคโทรไลท์ซึ่งช่วยควบคุมการโตของอนุภาคให้มีขนาดนาโนเมตร และป้องกันไม่ให้บริเวณพื้นผิวของอนุภาคเกิดปฏิกิริยาเคมีกับแก๊สออกซิเจนในอากาศ ซึ่งมีผลต่อความเข้มของแสงที่เปล่งออกมา สารเรืองแสงขนาดนาโนที่สังเคราะห์ได้นำไปตรวจสอบลักษณะโครงสร้างผลึก, ขนาดของผลึกและคุณสมบัติในการเปล่งแสง นำผลที่ได้มาเปรียบเทียบกับผลของสารเรืองแสงขนาดใหญ่หรือสารที่สังเคราะห์โดยไม่มีการเติมสารพอลิอิเลคโทรไลท์

ผลของการเลี้ยวเบนของรังสีเอ็กซ์ และภาพถ่ายจากกล้องจุลทรรศน์อิเล็กตรอนแบบส่องผ่านความละเอียดสูง พบริ้วการเลี้ยวเบนแลตทิซของอิเล็กตรอนของผลึกซิงค์ซัลไฟด์ ซึ่งแสดงลักษณะโครงสร้างผลึกเป็นแบบลูกบาศก์ มีขนาดประมาณ 2-3 นาโนเมตร ซึ่งในกรณีที่มีการเติมสารพอลิอิเลคโทรไลท์ลงในระบบพบว่าผลึกซิงค์ซัลไฟด์มีขนาดเล็กลง จากการวัดการเปล่งแสงของสารเมื่อถูกกระตุ้นด้วยพลังงานคลื่นแสงในช่วงเหนือม่วงและตามองเห็นได้ พบว่า สารเปล่งแสงในช่วงความยาวคลื่นประมาณ 600 นาโนเมตร ซึ่งตรงกับความยาวคลื่นแสงสีส้ม ทั้งนี้เกิดจากการเปลี่ยนระดับพลังงานของอิเล็กตรอนในแมงกานีสไอออนจาก $^4T_1$ (สถานะถูกกระตุ้น) ไปยัง $^6A_1$ (สถานะพื้น) และในกรณีที่มีการเติมสารพอลิอิเลคโทรไลต์พบว่ามีพีคการเปล่งแสงที่ความยาวคลื่นประมาณ 500 นาโนเมตรด้วย ซึ่งเกิดจากการเปลี่ยนระดับพลังงานของอิเล็กตรอนของสารพอลิอิเล็กโทรไลท์ ผลของการวัดความเข้มของแสงที่เปล่งออกมา พบว่าแสงที่เปล่งออกมามีความเข้มมากขึ้นเมื่อมีการเติมสารพอลิอิเลคโทรไลท์ลงในระบบ โดยมีความเข้มแสงสูงสุดเมื่อใช้ปริมาณสารพอลิอิเลคโทรไลท์ 4% w/v ผลของการวัดโดยเทคนิคฟูเรียทรานสฟอร์มสเปคโตรสโคปี(FTIR) และเทอร์มอลกราวิเมตริก อะนาไลซิส(TGA) ยืนยันว่ามีสารพอลิอิเลคโทรไลท์เคลือบที่ผิวของซิงก์ซัลไฟด์ที่เจือด้วยแมงกานีสไอออนโดยเกิดเป็นสารประกอบเชิงซ้อน

73 หน้า ISBN 974-04-5807-6

LIST OF CONTENTS

LIST OF CONTENTS (Continued)

LIST OF CONTENTS (Continued)

LIST OF TABLES

LIST OF FIGURES

LIST OF FIGURES (continued)

LIST OF FIGURES (continued)

LIST OF FIGURES (continued)

LIST OF ABBREVIATIONS

ZnS	=	Zinc sulfide
PL	=	Photoluminescence
EL	=	Electroluminescence
MPTS	=	3-methacryloxypropyl trimethoxysilane
PEL	=	Polyelectrolyte
PSSA-MA	=	Poly(4-styrenesulfonic acid-co-maleic acid)
E_{gr}	=	Ground state energy
E_{ex}	=	Excite state energy
T_d	=	Tetrahedral symmetry
^4G	=	First excited energy state of Mn^{2+} ion
VB	=	Valence band
CB	=	Conduction band
$^6A_1$	=	Energy ground state of Mn^{2+} ion
$^4T_1$	=	Energy first excited state in Mn^{2+} ion
O-D	=	Zero dimension
NC	=	Nanocrystal
β	=	Relative ratio of the radiative and nonradiative decay time (τ_R / τ_{NR})
D	=	Volume of a nanocrystal.
r	=	Nanocrystallite size
ε	=	Dielectric constant
m_e	=	Effective masses of the electron
m_h	=	Effective masses of the hole

LIST OF ABBREVIATIONS (continued)

DNC	=	Doped nanocrystal
MPTS	=	3-methacryloxypropyl trimethoxysilane
DDP	=	Di-*n*hexadecyldithiophosphate
PyDDP	=	Pyridinium di-*n*hexadecyldithiophosphate
C_s	=	Cluster surface
L	=	Ligand
CRTs	=	Cathode ray tubes
HDTV	=	High definition television
FED	=	Field emission display
ΔH	=	Enthalpy
k	=	Boltzmann's constant
T	=	Temperature
XRD	=	X-rays diffraction
D	=	Crystal diameter
B	=	Angular width
FWHM	=	Full width at half maximum
TEM	=	Transmission electron microscope
UV	=	Ultraviolet
Vis	=	Visible
FTIR	=	Fourier transform infrared spectroscopy
DSC	=	Differential scanning calorimeter
TGA	=	Thermal gravimetric analysis
XRF	=	X-ray fluorescence
ED	=	Electron diffraction

LIST OF ABBREVIATIONS (continued)

ΔE	=	Energy gap
h	=	Planck's constant.
c	=	Speed of light.
λ_{max}	=	Maximum absorption wavelength.

CHAPTER I
INTRODUCTION

Zinc sulfide (ZnS) nanocrystal has received a lot of attentions due to its excellent properties, such as a large energy band gap, direct recombination and resistance to a high electric field [1]. ZnS is categorized as a semiconductor material which is suitable for used as a host matrix for a large variety of dopants. ZnS doped with ions has attracted a lot of attentions from research community due to its versatile luminescence properties, such as photoluminescence (PL) [1-8], and electroluminescence (EL) [8,9]. An emission color of ZnS can be controlled by changing the choice of luminescent ion doping. For example, the doped of Mn^{2+} ion yields an orange emission ZnS:Mn^{2+} while doped with Cu^{2+} ion yields a green emission ZnS:Cu^{2+}. Some research, it was reported that by controlling a crystallized size of ZnS:Mn^{2+} to be in nanometer range can improve not only a higher luminescent efficiency but also a lifetime shortening from millisecond to nanosecond scale, in comparison with a bulk ZnS:Mn^{2+} [10-12]. A strong hybridization between the s-p states of the ZnS host and the states of the Mn^{2+} ion impurity which take places with a decreasing in crystallite size. This leads to both a decreased in a spin-forbidden character of the $^4T_1$-$^6A_1$ emission transition of Mn^{2+} ion and a faster energy transfer between the host and impurities, thus enhancing the efficiency of radiative recombination at the Mn^{2+} ion and shortening its decay time. These advantages make them used as the active layers of both alternating and direct current thin film electroluminescence devices [8,13,14] and ideal candidates as the fluorescent labeling agents, especially in biology [15,16].

Many methods have been used in the preparation of nanocrystalline ZnS:Mn^{2+} materials such as inverse micelle [17] and zeolites [18] often result in a very low yield of the particle thereby making their characterization difficult, consumption of expensive and environmentally unfriendly organic solvents. A directed synthesis of doped nanocrystals in aqueous solution is reported, by a liquid phase co-precipitation process [3,19-20]. In this method, organic and inorganic reagent can be used for

controlling the size of the crystals. In the presence of foreign molecules, crystal growth can be influenced by two different mechanisms, both intentionally and unintentionally: ions/molecules incorporated into the particle influence the precipitation/crystallization behavior and interacting with the crystal growth faces are control of the formation process [21]. Additionally, the sample obtained can be easily formed in large qualities or quantities relatively inexpensive means and doping of the nanocystal is easily possible at room temperature.

For ZnS:Mn^{2+} nanocrystalline materials, the surface states are very important to the optical properties. As the particles become smaller, the surface/volume ratio and the surface states is increased rapidly which leads to a surface defect and particles aggregation. These act as a non-radiative pathway for the excited electrons. To eliminate the non-radiative contribution from the surface states and particle aggregation, it is necessary to passivate the nanocrystal surface by using suitable capping or passivating agents. [4,11,19,22-26]. Lee and co-worker [19] reported the preparation of ZnS:Mn^{2+} nanocrystalline materials in the presence of 3-methacryloxypropyl trimethoxysilane (MPTS) as a surface-passivating on a photoluminescence. They found that a 30-fold enhancement was observed after the surface passivation. This was achieved by eliminating the surface defects on the nanocrystal surface. Bragava at. al [10] investigated the separation of the particles is maintained by coating with the surfactant methacrylic acid. In the coated ZnS:Mn^{2+} particle system they observed a gradual but significant increase in the luminescent intensity. However, it is still a challenge to develop in using passivating agent to produce ZnS:Mn^{2+} nanocrystals with good optical properties. One of interesting passivating agent is polyelectrolyte (PEL).

Natural polymer-based polyelectrolyte generally employed as thickeners or viscosity enhance simultaneously act as dispersing agents and stabilizers of colloidal systems due to increased viscosity as well as to intermolecular interactions with the suspended particles. In addition to, anionic PEL such as polyacrylic acid and acrylic acid copolymers were described for stabilizing coal suspensions for electrode manufacture, as well as for dispersing pigments in coating preparations and for stabilizing polymer lattices or suspensions of Al_2O_3 and SiC for a production of passivate the ZnS:Mn^{2+} nanocrystal surface.

In this work, the liquid phase co-precpitations process for synthesis nanocrystalline ZnS:Mn^{2+} is used. Poly(4-styrenesulfonic acid-co-maleic acid) (PSSA-MA), anionic PEL, was used as passivating agent for controlling a crystallization process and reduced surface defects. The effect of the PEL on the formation and optical properties of ZnS:Mn^{2+} nanocrystals will be investigated in this study.

CHAPTER II
OBJECTIVES

This study is aimed at studying the effect of Poly(4-styrenesulfonic acid-co-maleic acid) (PSSA-MA) as surface passivating agent on the crystal formation and optical properties of ZnS:Mn^{2+} materials. The results of the study are compared to those obtained from unpassivated and bulk ZnS:Mn^{2+} material. The reletionships between crystal size and optical properties of these materials are discussed.

In this work, the liquid phase co-precpitations process was used for nanocrystalline ZnS:Mn^{2+} synthesis where a doping of the nanocrystals is easily possible at room temperature. Additionally, organic passivating agent, PSSA-MA, was added into the reaction medium to control a crystallization process and reduce the surface defects. A condition of the experiment was adjusted by varying the amount of passivating agent. The synthesized samples were characterised by several techniques. The elemental analysis was used to investigate the presence of Zn-, S- and Mn-elements in the synthesized sample. The crystal strcture and size were determined by XRD and TEM. The optical properties were studied via photoluminescence properties and UV-Vis spectroscopy. In addition, the presence of PSSA-MA in the nanocrystalline sample was confirmed by FTIR and TGA.

The effect of surface passivating agent on the crystal formation, optical properties and the relationships between crystal size and optical properties of ZnS:Mn^{2+} materials will be discussed.

CHAPTER III

LITERATURE REVIEW

3.1 Luminescence [27]

There are several ways to excite a valence electron to a higher-energy state in the crystal. This can be done by the absorption of light or other radiation, or, for example, by a strong electric field. After a time interval ranging from microseconds to minutes, the electron returns to its ground state unless a photochemical reaction take place, for example, the formation of a latent image. The transition to the ground state must be accompanied by the dissipation of the extra energy. Usually part or all of the extra energy is dissipated as heat by interactions with the vibrating atoms in a crystal. Alternatively, the electron can lose its energy by the emission of a photon of light, according to the reaction

$$h\nu = E_{ex} - E_{gr} \quad (3.1)$$

when h is Planck's constant.

ν is frequency of light.

E_{ex} is excite state energy.

E_{gr} is ground state energy.

and the general process is called *luminescence* as show in figure below

.

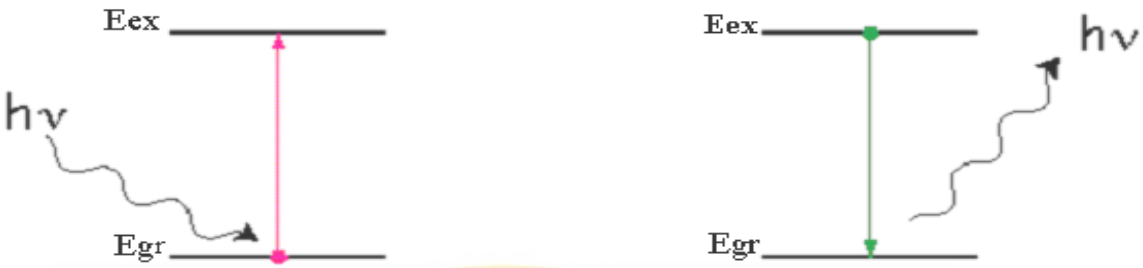

Absorption Luminescence

Figure 3.1 **A**bsorption and luminescence processes

Most crystals do not luminesce in their pure states. In fact, there is a great amount of evidence showing that luminescence occurs only when the crystal contains certain impurity atoms calls *activators*. Suppose an incident photon excites a valence electron from an activator atom to higher-energy state. The energy of the subsequencetly emitted photon is always less than the original excitation energy. The reason for this can be seen with the aid of Figure 3.2.

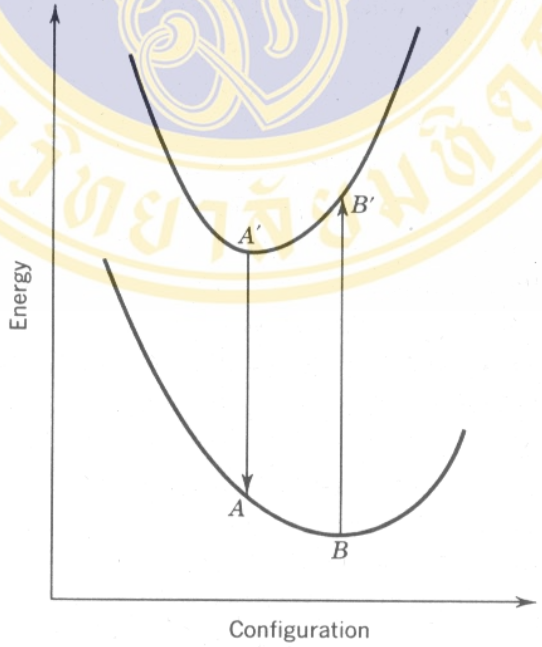

Figure 3.2 The energy diagram of characteristic luminescence proces

The ground state-energy as a function of the coordination of the activator atom is represented by the lower curve. When a photon is absorbed, it must expend energy sufficient for the transition B→B' to occur.

The configuration is charged by the excited electron since its orbital is now enlarged and alters the potential distribution in its vicinity. The energy dependence of the new situation is depicted by the upper curve in Figure 3.2. After reaching thermal equilibrium, the excited state has the energy corresponding to A′, so that, when the electron returns to its ground state, it undergoes a transition A′→A. The extra energies $E_{B'}$-$E_{A'}$ and E_A-E_B are expended as heat. It is clear from this discussion that the light emitted depends on the relative energies of the excited and ground states, so that it is characteristic of the activator atom. This process is; therefore, called characteristic luminescence. Because the emitted light has a longer wavelength, there is virtually no self-absorption of this light.

3.2 Luminescence type [27]

The different kinds of luminescence possible in crystals also depend on the means of employed to excite the electrons. Several categories can be distinguished, including:

3.2.1 Photoluminescence

Photoluminescence is a process in which the excitation is accompanied by the absorption of photons. The radiation source may be infrared, visible, ultraviolet, or X-radiation; for example, this is the way that incident radiation is made visible in phosphorescent coating used in x-ray fluoroscopy and infrared-image converters.

3.2.2 Cathodoluminescence

Cathodoluminescence results when a phosphor is bombarded by high energy electrons or cathode rays. This is the process that takes places in the screens of cathode-ray tubes and television tubes.

3.2.3 Electroluminescence

Electroluminescence occurs when a phosphor is placed in an insulating medium having a very high dielectric constant and an alternating electric field is applied across the crystal. The very large electric-field strength build up inside the phosphor is sufficient to "empty" an activator quantum state. When the excited electron subsequently returns to its ground state, visible light is emitted. The light given off is a function of voltage and frequency of the applied field. It is similarly possible that future television screens will use electroluminescence rather than cathodoluminescence in television sets that will hang like pictures on a wall.

3.2.4 Thermoluminescence

The electrons are not initially excited by thermal means. Instead, the electron are excited by other means at very low temperature and become trapped in states lying in the forbidden-energy region. The low temperature regards the emptying of these states, so that luminescence does not occur until the temperature of the phosphor is subsequently increased.

3.2.5 Triboluminescence

Triboluminescence is produced when two fairly hard insulators, for example, two quarlzite rocks, are briskly rubbed together.

3.3 Luminescence material

3.3.1 Structure of cubic ZnS crystallizes [28]

ZnS crystallizes as cubic closest-packed array of S^{2-} ions with Zn^{2+} ions in tetrahedral holes. The figure 3.3 shows that the tetrahedral holes in a face-centered cubic unit cell are in the corners of the unit cell, at coordinates such as 1/4,1/4,1/4. An atom with these coordinates would touch the atom at this corner as well as the atoms in the centers of the three faces that form this corner.

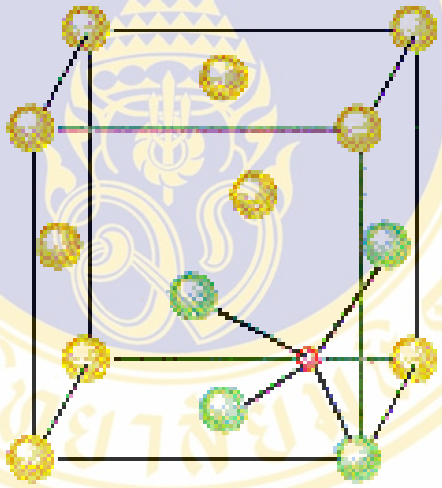

Figure 3.3 The tetrahedral holes in a face-centered cubic unit of ZnS crystal.

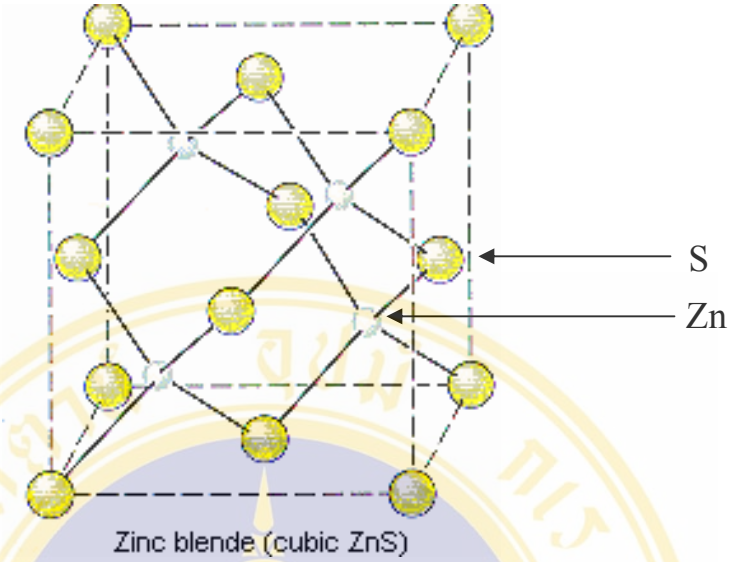

Figure 3.4 The face-centered cubic unit cell of ZnS crystal.

Because the corners of a cubic unit cell are identical, there must be a tetrahedral hole in each of the eight corners of the face-centered cubic unit cell. The unit cell of ZnS shown in the figure 3.4. S^{2-} ions occupy the lattice points of a face-centered cubic unit cell and Zn^{2+} ions are packed into every other tetrahedral hole. The cell-edge length is 0.5411 nm.

3.3.2 Zinc sulfide doped with activator ions [27]

The role that an activator ion plays in a phosphor depends on its position in the crystal structure. If it occupies a substitution position, that is, when it is in a correct metal site, it behaves differently than when it is incorporated interstitially.

Zinc sulfide doped with activator ions is known to have efficient light emitting properties, especially Mn^{2+}-doped ZnS. The identical ionic states of the migrating Mn^{2+} and host lattice Zn^{2+}, their ionic radii are also similar, i.e., 0.83 Å (Zn^{2+}) and 0.80 Å (Mn^{2+}). It is therefore anticipated that Mn^{2+} migration takes place by the simultaneous replacement of Zn^{2+}, i.e., partial substitution of ZnS with MnS. [29]

When Mn^{2+} ions act as efficient luminescent centers are substituted for some Zn^{2+} ones in a ZnS crystal, the ^4G of the first excited state of Mn^{2+} in tetrahedral symmetry, T_d, is split. Because of the crystal-field disturbance, the effect of other ions around on the electronic structure of Mn^{2+} ions relieves some forbidding. Then, the crystal field transition of Mn^{2+} is strongly dependent on its host crystal structure.

The Mn^{2+} ion has a $3d^5$ electronic configuration. The ground state of the $3d^5$ configuration is the sextet $^6A_1$ with the total spin 5/2. The first excited level is the triplet states $^4T_1$, which is the excited state closest to the ground state. We are interested in the optical transition between the first excited state and the ground state; this is the transition $^4T_1 - ^6A_1$ which gives an orange emission which is characteristic emission of Mn^{2+} in the ZnS , following Figure 3.5.

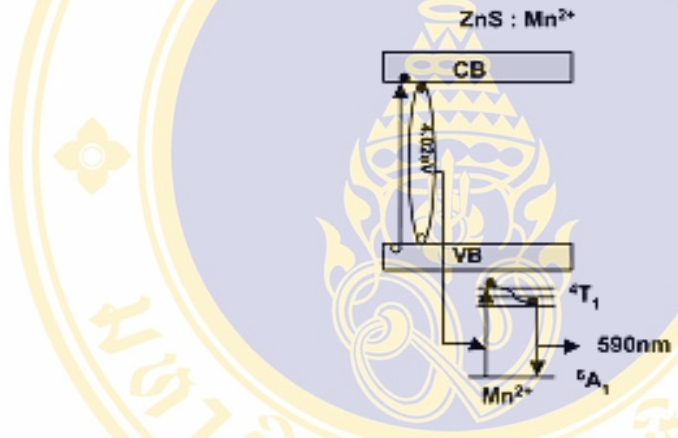

Figure 3.5 The schematic band diagram of zinc sulfide doped with Mn^{2+} [30].

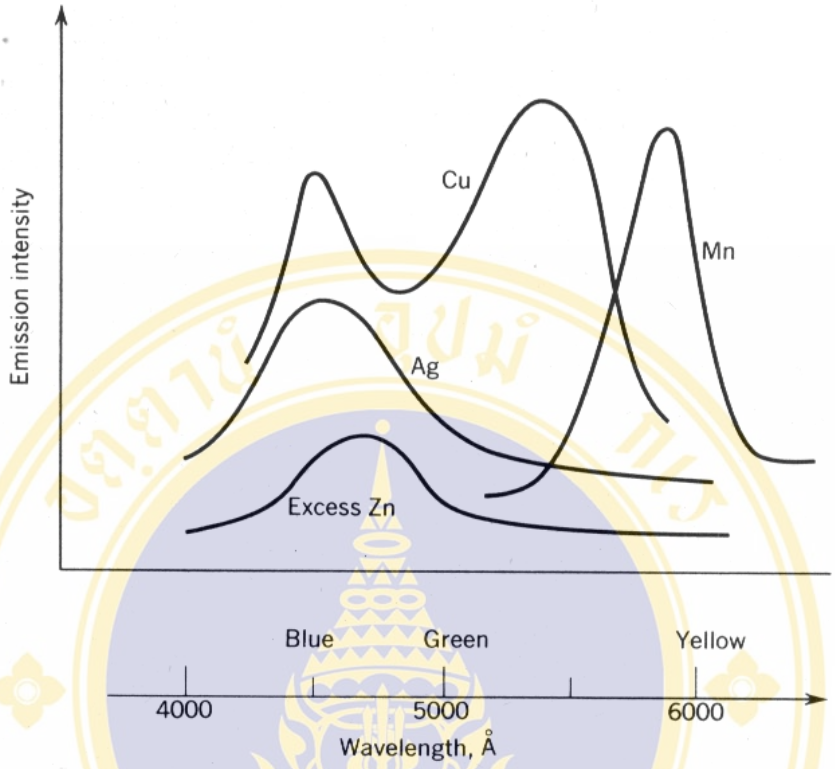

Figure 3.6 Luminescence spectra of zinc sulfide activated with Mn, Cu, Ag and excess zinc, stimulated by ultraviolet light. The vertical scales of each curve are expressed in arbitrary units to facilitate their comparison. [27].

An emission color of ZnS can be controlled by changing the choice of luminescent ion doping. Figure 3.6 shows the emission curves of ZnS activated with manganese ion and compare with different activator ions such as copper, silver, and excess zinc. The divalent manganese ions substitute for divalent zinc atoms and emit yellow-orange light, the blue light emitted when Cu^{1+}, Ag^{1+}, or excess zinc is incorporated in the crystal is believed to be caused by transition between energy states introduced in the forbidden-energy region by vacancies present in the crystal. On the other hand, the pronounced green emission, when copper is incorporated, is attributed to divalent copper atoms substituting for zinc.

3.4 A nanocluster or nanocrystal [31]

A *nanocluster* or *nanocrystal* is a fragment of solid comprising somewhere between a few atoms and a few tens of thousands of atoms. Over the past ten years huge advances have been made both in the synthesis of size-tunable, monodisperse nanoclusters of various chemical compositions and in the development of techniques for their assembly into well-ordered nanostructured solids (facilitating the synthesis of what have been termed 'designer materials').

This is largely due to the very high surface-to-volume ratio in nanoclusters. For example, a 1000-atom cluster will generally have approximately 25% of its atoms at the surface. This in turn means that free nanoclusters have a high density of unsatisfied, dangling bonds and, correspondingly, high surface free energies. The surfaces of bulk inorganic semiconductors (for example, III–V, II–VI compounds and group IV (Si, Ge) elements) generally reconstruct. High surface free energies also mean high cluster reactivities. Hence, a semiconductor cluster prepared under high-vacuum conditions will readily oxidize on exposure to the atmosphere. Again, this generally significantly degrades the electrical and optical properties of the cluster. For metallic clusters and, in particular, ferromagnetic clusters where the spin state of the cluster will be dramatically affected by contamination, oxidation and aggregation of nanoclusters created under (ultra) high vacuum and exposed to ambient conditions are particularly acute problems.

Presently, several nanocrystalline particle systems have been studied as a free standing powder or in a matrix. The main goal of these studies has been to understand the physical properties of these quantum confined O-D nanocrystals. The practical photonics applications of these nanocrystals are still lacking due to the fact that the surface-related nonradiative recombination dominates in the strong confinement limit. Additionally, different applications of these nanocrystals in a device have yet to be demonstrated. To eliminate the non-radiative contribution from the surface states, one needs to passivate the free standing quantum dots.

3.5 Surface passivation

Passivation of the cluster surface, i.e. the termination of cluster dangling bonds with either an organic or inorganic addend, significantly reduces the chemical reactivity of the cluster and, for semiconductor clusters, may lead to a reduction in mid-gap states. Perhaps a more significant consequence of termination of the cluster surface is that the correct choice of addend can lead to an effective functionalization of the cluster. That is, intercluster interactions can be mediated by, for example, organic ligands.

The surface passivation can be achieved in several ways. They are:

(i) Nanocrystals (NC) suspended as colloidal particles in a liquid

(ii) NC formed in matrix such as glass or polyethylene film

(iii) NC in a cage such as zeolites

(iv) Individual NC coated with a passivating layer such as methacrylic acid.

The passivation reduces the non-radiative contribution of the surface and enhances the luminescent efficiency.

3.6 Optical properties of Mn^{2+}-doped ZnS nanocrystal materials

Optical properties of semiconductor nanocrystallites have been investigated extensively in recent years**,** since these materials have potential application to optical devices and their optical properties different from the corresponding bulk crystals [6, 10]. Most work has been devoted to understanding the intrinsic optical properties of such materials.

More recently, the optical properties of impurities such as transition metal ion doped semiconductor nanoparticles have been studied, in particular, Mn^{2+}-doped ZnS nanocrystals[11-12]. The optical properties of nanocrystalline material relate to the crystallite size, band gap, and nanocrystal growth control by surface passivation will be discussed more in details.

3.6.1 The size dependence of optical properties

Bhargava et al. [10] first synthesized ZnS semiconductor nanocrystallites doped with Mn^{2+} ions and investigated its size dependence of optical properties. They found that the photoluminescence of Mn^{2+} ions in ZnS nanocrystals had a very high quantum efficiency with a luminescence decay several orders of magnitude faster than in the bulk crystals.

They studied the optical properties of passivated nanocrystalline ZnS:Mn^{2+} which were prepared by an organometallic reaction at room temperture. The doped nanocrystalline's, ranging in size from 35 to 70 Å, were passivated using monomer to prevent agglomeration. The surface passivated quantum dots were characterized optically for their efficiency. They suggest that the room-temperature quantum efficiency was observed to be dependent on the size of the nanocrystal, increasing from < 1% at 70 Å to > 20% at 3.5 Å. They suggested that the luminescence efficiency [10], η, in the nano-particle can be expressed as

$$\eta = \frac{1}{\left(1 + \beta D^2\right)} \tag{3.2}$$

where β is relative ratio of the radiative and nonradiative decay time (τ_R / τ_{NR}) and, D is the volume of a nanocrystal. From equation (3.2), it indicates that the luminescence efficiency of the nanocrystals will be increase when crystallite size decreases as shown in Figure 3.7.

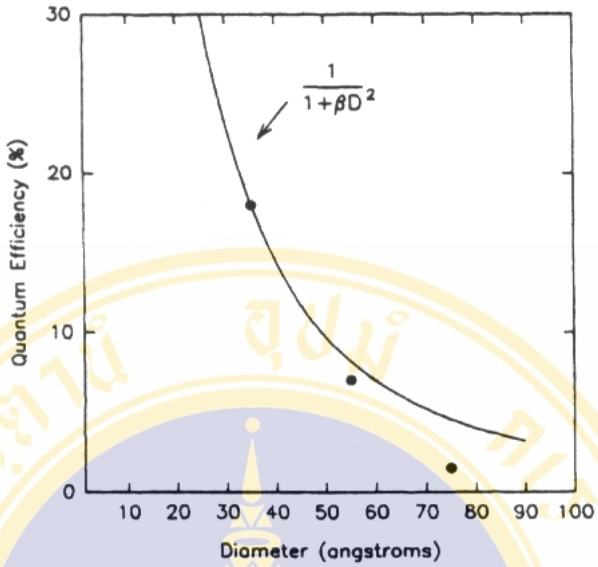

Figure 3.7 A variation of the external luminescent efficiency as a function of the size of the nanocrystals.

3.6.2 Optical properties related to band gaps

The theoretical band gap shift (ΔE) based on the effective mass approximation [32] is defined as:

$$\Delta E = \frac{h^2\pi^2}{2r^2}\left[\frac{1}{m_e}+\frac{1}{m_h}\right]-\frac{1.786e^2}{\varepsilon^R}-\frac{0.248e^4}{2\varepsilon^2h^2}\left[\frac{1}{m_e^{-1}+m_h^{-1}}\right] \qquad (3.3)$$

where ***r*** is the nanocrystallite size, ε, the dielectric constant, and m_e, and m_h are effective masses of the electron and hole, respectively. The first term in the equation corresponds to the kinetic energy, the second term, to the Coulomb energy, and the third term is attributed to the correlation effect. The size dependent shift of the band gap in nano-crystals can be estimated within the limit of the effective mass theory [33].

Yu et al. [7] studied the optical properties of Mn-doped ZnS nanoparticles having different crystallize size. They found that the blue shift in optical band gap by 0.34-0.41 eV with the decrease in the crystallite size by 0.4 nm.

3.6.3 Effect of Surface passivation on optical properties

Jin et al.[34] observed the influence of the surfactant (polymethyl methacrylate) on the Mn^{2+} luminescence of ZnS:Mn nanocrystals. It was found that the Mn^{2+} luminescent intensity is enhanced several or tens of times that of samples without surfactants. This similar sample was explained by Lu SW [19]. They found that a 30-fold increase in photoluminescence intensity after surface passivation by a passivating agent with 3-methacryloxypropyl trimethoxysilane (MPTS). Additionally, Chen et. al. [35] prepared ZnS nanoparticles coated with di-*n*hexadecyldithiophosphate (DDP). They found that the existence of DDP coating on the surface of the ZnS nanoparticles, water adsorption and oxidation were prevented and thermal stability of DDP coating on ZnS nanoparticles was superior to that of pyridinium di-*n*hexadecyldithiophosphate (PyDDP).

Poly(4-styrenesulfonic acid-co-maleic acid) (PSSA-MA), sodium salt

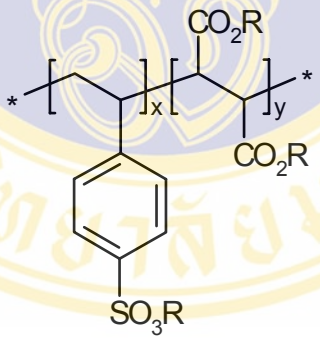

R and R′ = Na^+

Figure 3.8 Molecular structure of poly(4-styrenesulfonic acid-co-maleic acid)(PSSA-MA), sodium salt.

Poly(4-styrenesulfonic acid-co-maleic acid)(PSSA-MA), sodium salt is anionic polyelectrolyte. It contains two different functional groups: –COOH and $–SO_3H$ as shown in Figure 3.8. Carboxyl groups, two per each constitutional repeating unit, are bonded on two neighboring carbon atoms of the copolymer backbone, weakly dissociated in aqueous solution, unequal in strength but characterized by the strong interaction. Sulfonate groups are located several bonds away from the copolymer backbone, and they are completely dissociation in aqueous solution. As both groups

differ in hydration, they are surrounded by a different structure of water molecules [36].

In this study, PSSA-MA was chosen as a surface passivation agent for Mn^{2+}-doped ZnS nanocrystals, which have a potential to enhance PL.

3.7 Theory of nucleation and growth process of nanocrystal within organic additive [37]

Velex et al. [38] has had considerable success in preparing a range of inorganic particles of controlled size and shape by judicious control of nucleation and growth processes. Other examples of biomimetic strategies include the use of soluble organic additives such as polyelectrolytes, block copolymers, and biopolymers to either inhibit or modify the crystallization process [34,39-40].

It is important to understand how these processing parameters influence the nanocluster growth process. Understanding the growth process and why the growth stops at a particular nanocluster size is essential for developing a rational synthesis of semiconductor nanoclusters within organic additive. It is assumed in Cohen et.al [36] that the nanoclusters are stabilized by interactions between the nanocluster surface and polymer ligands (such as carboxylic acid groups present in the polymer microdomains). The interaction can be considered to be a reversible reaction between the ligand (L) and the cluster surface (Cs), with (#LCs) representing the number of cluster-ligand bonds.

$$L + Cs \leftrightarrow LCs \tag{3.4}$$

Nanocluster growth stops when $(\#LCs)_r$ cluster-ligand bonds of the reversible reaction are formed and trap the nanoparticle in an energy well. If ΔH is the enthalpy change on the formation of a ligand-cluster bond, an alternate way of stating this constraint is that growth stops when

$$-(\#LCs)_r \Delta H >> kT \tag{3.5}$$

At the same time, for a nanoparticle of a certain size at a certain temperature, there will be an equilibrium number of cluster-ligand bonds $(\#LCs)_{eq}$. If $(\#LCs)_r > (\#LCs)_{eq,}$ nanoparticle stabilization will not take place, and growth will continue. To explain the stabilization at a particular particle size, two models may be invoked. The first one is a reaction-diffusion model, which implies a competition between a reaction time (time required to form $(\#LCs)_r$ cluster-ligand bonds) and a diffusion time (time required for particles to collide and coalesce). Growth stops when the diffusion time is greater than the reaction time. The second possible model is an equilibrium model, which would be valid if the cluster-ligand reaction is fast but if $(\#LCs)_r$ is initially greater than $(\#LCs)_{eq}$. In this case, growth will proceed until the nanoparticle reaches a size for which $(\#LCs)_r \leq (\#LCs)_{eq}$.

3.8 Application of doped nanocrystal (DNC) materisls [11]

Several applications of doped nanocrystal (DNC) materials are being developed by nanocrystals technology. They were reported by Bragava et al [11]. In brief, they exploit the following key properties of DNC for various technological applications: (a) high absorption, (b) high efficiency, (c) ultrafast speed and (d) ultra-high density. Some of the applications are:

Displays: The rare-earth and transition metals yield efficient phosphors. In active displays such as CRTs, we need high intensity without light saturation for next generation high definition TV (HDTV). Since DNC phosphors are expected to be superlinear phosphors due to its ultrafast luminescent recombination speed, saturation for HDTV can be eliminated. In the case of a flat-slim display such as the Field Emission Display (FED), the DNC phosphors can be excited at much lower voltages (~1 kV), which results in a reduced TV-depth from 18″ to 0.5″. Other potential applications would be in plasma and electroluminescent displays.

Sensors: The DNC particles can yield ultrafast sensors since the transfer rate from the host to quantum dots is < 20 ps. These ultrafast sensors could be also used for X-ray, γ-ray detection and as a fast scintillator phosphor. Future DNC materials may be used as photoelectric (solar-cells) sensors.

Lasers: The impurity in the DNC materials retains its own atomic levels within the band gap of the host DNC material. Since the carrier trapping to these impurity states is fast compared to recombination times in DNCs, these states could be consider as intrinsic part of the DNC host states. This combined host and impurity energy levels scheme. An additional advantage these doped nanocystalline materials possess over other hosts that the high density of states of the host preventing the excited state absorption in the rare-earth. This absorption within the hosts provides a large excitation cross-section and simultaneous rapid transfer to the impurity. We believe that a new class of lasers will be fabricated from these doped quantum dots.

There are many other applications which involve implementation of these DNC materials directly in systems. The key issue remains how to fabricate device structures from DNC materials with can be directly incorporated in present systems. To achieve these in a cost-effective manner, new processes will have to be developed to handle these ultra-small particles. The potential applications of these doped nanocrystalline materials have yet to be exploited. The “caged atom” in a nanocrystal behaves like a “frozen gas”. This suggests that the plasma-like conditions can be achieved in DNC materials at room temperature. It should be noted that the size of these particles are similar to the size of critical components of the biological systems. Thus, by studying DNC materials, they may begin to unravel the physics of the biological systems [41], a major goal for the materials scientists in the 21st century.

CHAPTER IV

MATERIALS AND METHODS

4.1 Chemicals

The chemicals used for synthesis of the ZnS:Mn^{2+} nanocrystals are listed in Table 4.1

Table 4.1: List of chemicals

Chemicals	Suppliers
Zinc acetate dihydrate $(CH_3COO)_2$ Zn.$2H_2O$) 95.5%	Ajax Finechem
Manganese(II)acetate tetrahydrate $(CH_3COO)_2$ Mn.$4H_2O$) >99%	Fluka, Switzerland
Sodium sulfide nonahydrate >98%	Sigma, USA
Poly(4-styrenesulfonic acid-co-maleic acid)(PSSA-MA), sodium salt	Aldrich Chem. Co., USA.
Methanol technical grade	Reagent Chemical Industry LTD, Thailand
Deionized water	Central Instruments Facility (CIF)

4.2 Synthesis of ZnS:Mn^{2+} nanocrystals with and without passivating of PSSA-MA

$ZnS:Mn^{2+}$ nanocrystals were prepared by a liquid phase co-precipitation process. To prevent the side reactions, the reaction was carried under an inert atmosphere (N_2), 50 ml methanoic solution of 0.2 M zinc acetate dehydrate ($Zn(CH_2COO)_2.2H_2O$) and 0.004 M manganese acetate tetrahydrate ($Mn(CH_2COO)_2.4H_2O$) were mixed together with poly(4-styrenesulfonic acid-co-maleic acid) (PSSA-MA) by varying the concentration of PSSA-MA in the water from 0 to 8 wt%. The reaction was stirred with a magnetic stirrer to yield a mixed solution. A 20 ml aqueous solution of 0.5 M sodium sulfide ($Na_2S.9H_2O$) was added immediately and the reaction was stirred for 24 hour. The precipitate was separated by centrifugation at 4000 rpm for 20 min, then washed with methanol and deionized water several times. The product of $ZnS:Mn^{2+}$ nanocrystals were kept in aqueous solution. The samples used in this study have two forms: powder and colloid.

The reactions take place as followed:

1) $ZnS:Mn^{2+}$ nanocrystals

$$Zn(CH_2COO)_2.2H_2O + Mn(CH_2COO)_2.4H_2O) + Na_2S.9H_2O \rightarrow ZnS:Mn^{2+} + 2Na(CH_2COO)_2$$

2) $ZnS:Mn^{2+}$ nanocrystals passivated with PSSA-MA

$$Zn(CH_2COO)_2.2H_2O + Mn(CH_2COO)_2.4H_2O) + Na_2S.9H_2O + PSSA\text{-}MA \rightarrow ZnS:Mn^{2+} + 2Na(CH_2COO)_2 + PSSA\text{-}MA$$

4.3 Geometrical and crystallographical properties

The white cloudy solution of $ZnS:Mn^{2+}$ nanocrystals were dried eventually at 80^oC to remove solvents. The powder of $ZnS:Mn^{2+}$ nanocrystals were obtained. The nanocrystal powder was characterized by the following techniques.

4.3.1 X-rays diffraction (XRD)

A crystalline of ZnS:Mn^{2+} exhibit Bragg diffraction peaks in X-ray diffraction measurements. However, due to their small size, a fine particle broadening is observed in Bragg diffraction peaks. A condition for constructive reinforcement for X-ray scattering from crystalline solid is given by Bragg's law as shown in equation 4.1

$$2d \sin\theta = n\lambda \qquad (4.1)$$

This explains the path difference of X-rays scattered from parallel crystalline plane space, $d = d_{hkl}$ apart to an integral (n) number of X-ray wavelengths λ. θ is a X-ray angle of incidence (of δ-diffraction) measured with respect to the crystalline planes. For an infinite crystal Bragg scattering occurred at discrete values of 2θ satisfies the Bragg condition, i.e. Bragg peaks are function. For a finite sized crystal (in Figure 3.1) the peaks are broadened over a range of angles.

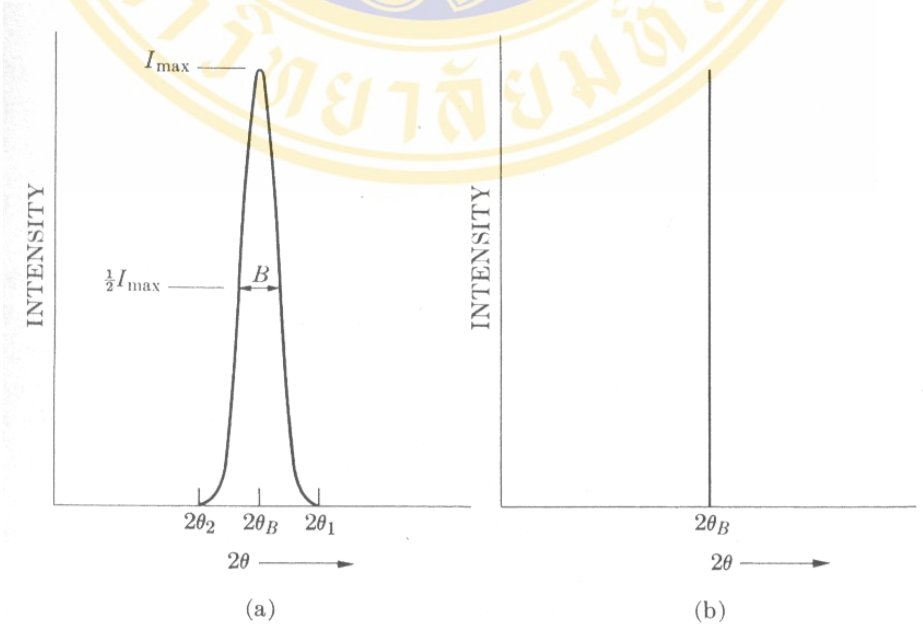

Figure 4.1 The effect of fine particle broadening in XRD (a) fine particle and (b) perfect crystal. [42]

The phenomenon of fine particle broadening was explained by B.D. Cullity [42]. They consider a finite crystal of thickness, $t = md$, where m is an integer, and d is the distance between crystalline phases, i.e., there are m planes in t. The width of the diffraction curve of figure 4.1 increases as the thickness of the crystal decrease, because the angular range ($2\theta_1 - 2\theta_2$) increases as m decreases. The width B is usually measured, in radians, at an intensity equal to half the maximum intensity.(Note that B is an angular width, in terms of 2θ (not θ), and not linear width.) As a rough measure of B, we can take half the difference between the two extreme angles at which the intensity is zero, which amounts to an assuming that the diffraction line is a triangular in shape. Therefore,

$$B = \frac{1}{2}(2\theta_1 - 2\theta_2) = \theta_1 - \theta_2 \qquad (4.2)$$

The path-difference equations for these two angles can be written similar to Bragg equation, Eq. (4.1), but related to the entire thickness of the crystal rather than to the distance between adjacent planes:

$$2t \sin\theta_1 = (m+1)\lambda ,$$

$$2t \sin\theta_2 = (m-1)\lambda .$$

By subtraction we find

$$t(\sin\theta_1 - \sin\theta_2) = \lambda ,$$

$$2t \cos\left(\frac{\theta_1 + \theta_2}{2}\right)\sin\left(\frac{\theta_1 - \theta_2}{2}\right) = \lambda .$$

But θ_1 and θ_2 are both very nearly equal to θ_B, so that

$$\theta_1 + \theta_2 = 2\theta_B \quad \text{(approx.)}$$

$$\sin\left(\frac{\theta_1 - \theta_2}{2}\right) = \left(\frac{\theta_1 - \theta_2}{2}\right) = \lambda . \text{ (approx.)}$$

Therefore

$$2t\left(\frac{\theta_1 - \theta_2}{2}\right)\cos\theta_B = \lambda ,$$

$$D = \frac{\lambda}{B \cos \theta_B} \tag{4.3}$$

A more exact treatment of the problem gives

$$D = \frac{0.9\lambda}{B \cos \theta} \tag{4.4}$$

which is known as the Scherrer formula. It is used to estimate the *particle size* of vary small crystals from the measured width of their diffraction curves.

Where D is the crystal diameter (Å)

λ is the wavelength of Cu Kα radiation (1.54 Å)

B is the full width at half maximum (FWHM) of XRD peaks (radian)

θ is the diffraction angle

The nanocrystal powder was placed in an aluminium holder for a crystal structure investigation. Information on structure and crystal size of the nanocrystal was obtained from a Bruker D8 X-ray powder diffractrometer. The XRD spectra were collected in the step scan mode typically with 2θ data collection and using step increments in the angle of 0.02 degree over 2θ range 10º to 70º. The accelerating voltage and current were 40 kV and 30 mA, respectively, for Cu Kα radiation ($\lambda_{K\alpha}$ = 1.542 Å). The size of nanocrystal was determined from the full width at half maximum (FWHM) of XRD peaks via the Scherrer formular.

4.3.2 Transmission Electron Microscope (TEM)

Microscopic structural information was obtained by using a JEOL JEM 2010 transmission electron microscope (TEM) operating at 200 KV. For TEM sample, were prepared by dispersing the as-prepared ZnS:Mn^{2+} nanocrystals in acetone, picking up the nanocrystals film on carbon coated copper grid. The sample was kept in desiccator prior to an investigation.

4.4 Properties related to band gap

The absorption study is important to identify the crystallite size, size distribution and energy gap of ZnS:Mn^{2+} nanocrystal. For UV-Vis absorption spectra of ZnS:Mn^{2+} nanocrystal disperse solutions were recorded by using a JENWAY 6405 UV-Vis spectrophotometer. The light sources cover both UV and visible range, 190 to 1,100 nm. In this experiment, wavelength from 200 to 700 nm was used and its specification is shown in Table 4.2.

Table 4.2: Specification of UV-Vis Spectrophotometer

Model	6405
Light source	Deuterium
Output	Analogue/RS232 serial port
Wavelength	190-950 nm
Resolution	0.1 nm
Bandwidth	5 nm
Maximum Scan Speed	1400 nm/min

4.5 Photoluminescence Properties

Photoluminescence spectra of ZnS:Mn^{2+} nanocrystal powder and solution were observed by using the Ocean Optics spectrometer. The experiment setup for measurement spectra of light consists of UV-Vis light source, fiber optics, and USB 2000 spectrometer. The spectrometer and the data collection were controlled by a personal computer. The experimental set up for emission spectra is shown in Figure1A in Appendix A.

The UV-Vis light source with wavelength of 385 nm was used to excite the sample for photoluminescence measurement.

4.6 ZnS:Mn^{2+} nanocrystal surface

The absorption of polyelectrolyte on ZnS:Mn^{2+} nanocrystal surface was confirmed by Fourier Transform Infrared (FTIR) spectra. Perkin Elmer GX spectrophotometer in the 4000-370 cm^{-1} region and sixteen scans at a resolution of 4 cm^{-1} was used. ZnS:Mn^{2+} nanocrystal powder (0.5-1.0mg) is mixed with approximately 100 mg of dry, powdered KBr. Mixing can be effected by thorough grinding in a smooth agate mortar. The mixture is pressed with special dies under a pressure of 2000 psi into a transparent disk.

4.7 PSSA-MA content in sample

The percent content of PSSA-MA polyelectrolyte in sample was measured by using STD 2960 simultaneous differential scanning calorimeter (DSC) and thermal gravimetric analysis (TGA), from room temperature up to 1000^{o}C in an inert N_2 gas and the heating rate of 20^{o}C/min.

4.8 Elemental analysis

The presence of manganese in ZnS nanocrystals and also the amount of Mn^{2+} in each ZnS sample were confirmed by using S4 Explorer X-ray fluorescence (XRF). The sample was prepared by pressed-disk. ZnS:Mn^{2+} nanocrystal powder is pressed with special dies under a pressure of 2000 psi and a cloudy disk was obtained.

CHAPTER V
RESULTS AND DISCUSSION

In this study, the $ZnS:Mn^{2+}$ nanocrystalline substances were synthesized and characterized for various applications, e.g., electroluminescent materials, phosphor, and other light emitting materials[8,13-16]. The nanocrystals were synthesized by liquid phase co-precipitation method with adding poly(4-styrenesulfonic acid-co-maleic acid) (PSSA-MA) as passivating agent. The effect of passivating polymer on the crystallized size and the optical properties will be investigated in this study.

5.1 Geometrical and crystallographical properties

5.1.1 XRD patterns and crystal size of nanocrystalline ZnS:Mn^{2+}

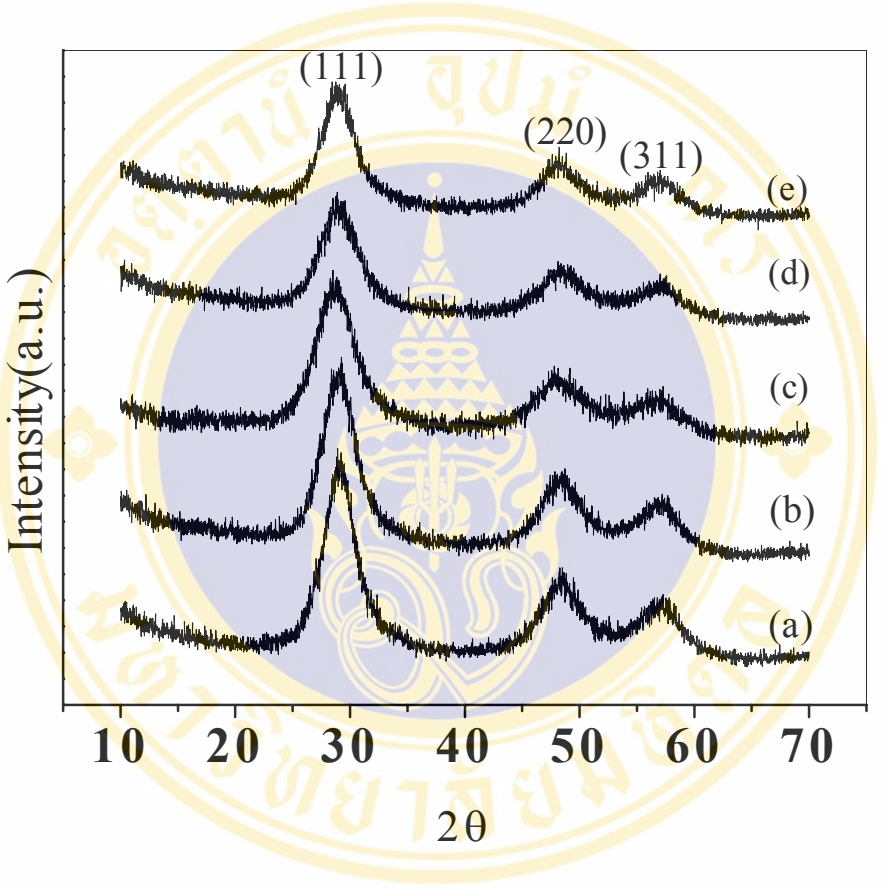

Figure 5.1 X-ray diffraction pattern of ZnS:Mn^{2+} nanocrystalline powder passivated with PSSA-MA (a) 0% w/v, (b) 2% w/v, (c) 4% w/v, (d) 6% w/v, and (e) 8% w/v respectively.

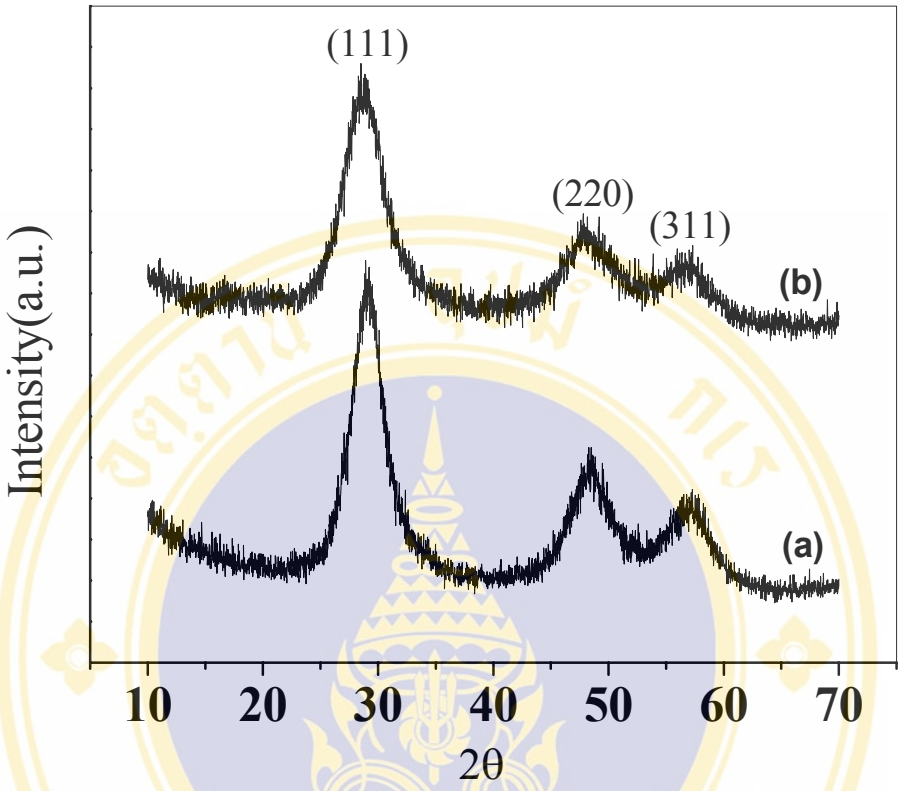

Figure 5.2 X-ray diffraction pattern of ZnS:Mn^{2+} nanocrystalline powders passivated without (a) and with PSSA-MA (b).

Powder X-ray diffraction (XRD) patterns for ZnS:Mn^{2+} nanocrystalline materials passivated with PSSA-MA 0-8% w/v are shown in Figure 5.1 (a-e). The crystal structure and size of nanocrystalline were obtained from X-ray diffraction peaks. Three broad diffraction peaks are at 2θ of 28.4^{o}, 48.6^{o} and 58.6^{o} which correspond to (111), (220) and (311) planes, respectively. They are matched with a cubic (zinc blende phase) for all samples. Due to the reduction in crystallize size, the XRD peaks are broadening which can be observed as an increase in the width of the diffraction peak. A comparison between unpassivated and passivated with PSSA-MA is shown in Figure 5.2 (a) and (b), respectively. These results clearly indicate that very small nanocrystals are present in the samples. The samples passivated with PSSA-MA show broader peaks than those of unpassivated. From the width of XRD peak

broadening, the crystal size of ZnS:Mn^{2+} can be calculated by using the FWHM via the Debye-Scherrer formula:

$$D = \frac{0.9\lambda}{B \cos \theta} \tag{5.1}$$

Where D is the crystal diameter (nm)

λ is the wavelength of x-ray radiation (1.54 Å)

B is the full width at half maximum of XRD peaks (radian)

θ is the diffraction angle

Thus, for example

Suppose λ=1.54 Å, $B = 6.05 \times 10^{-2}$ radian (XRD peak of (111) plane) and θ=28.96°.

$$D = \frac{0.9 \times 1.54}{6.05 \times 10^{-2} \times \cos 28.96^{\circ}} = 2.62 \text{ nm}$$

Table 5.1 List of crystallized size of all synthesized samples.

Sample	Crystal size(nm) (111)
$ZnS:Mn^{2+}$	2.70
$ZnS:Mn^{2+}$_PSSA-MA 2% w/v	2.63
$ZnS:Mn^{2+}$_PSSA-MA 4% w/v	2.24
$ZnS:Mn^{2+}$_PSSA-MA 6% w/v	2.42
$ZnS:Mn^{2+}$_PSSA-MA 8% w/v	2.68

Table 5.1 shows crystal size of unpassivated and passivated $ZnS:Mn^{2+}$ with PSSA-MA 2-8% w/v. It shows that the crystal size of passivated samples is smaller than that of unpassivation which corresponds to broadening of XRD peak. These results indicate that the crystal growth of $ZnS:Mn^{2+}$ was inhibited by PSSA-MA polyelectrolyte.

5.1.2 TEM images and electron diffraction pattern of nanocrystalline $ZnS:Mn^{2+}$

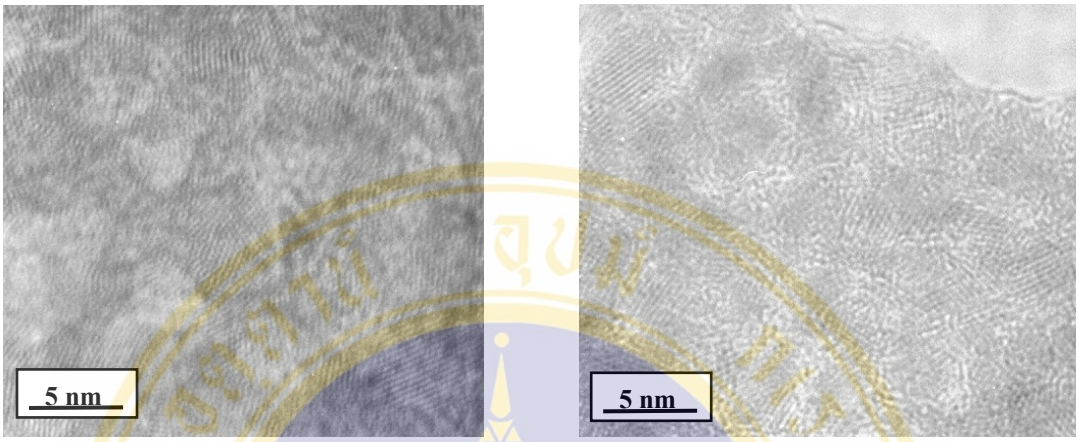

(a) **(b)**

Figure 5.3 High resolution TEM images of nanocrystalline $ZnS:Mn^2$ with (a) and without (b) a passivating of PSSA-MA.

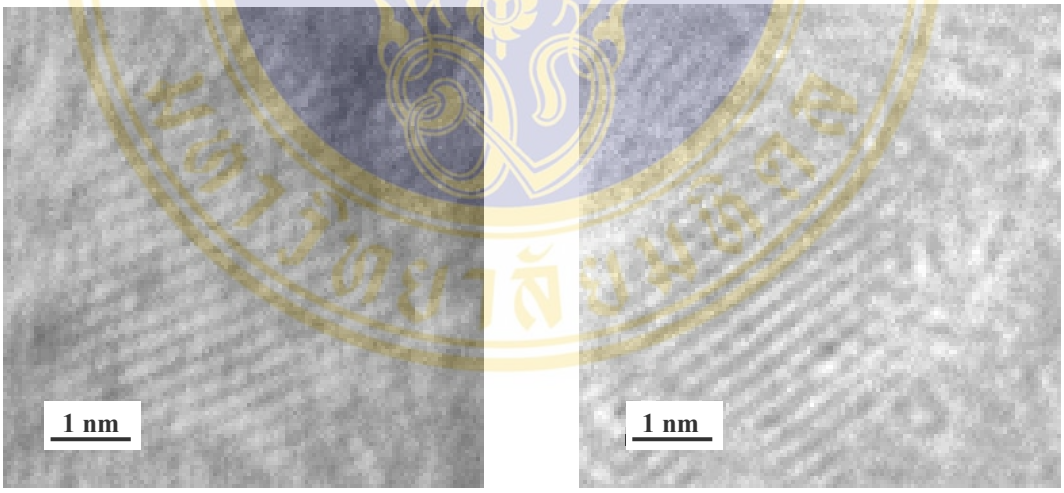

(a) **(b)**

Figure 5.4 High resolution TEM images of an individual $ZnS:Mn^{2+}$ nanocrystal with (a) and without (b) a passivating of PSSA-MA.

The morphologies and crystal size of the ZnS:Mn^{2+} nanocrystals were observed by TEM which is a tool to confirm the results obtained from XRD. Figure 5.3 (a) show high resolution TEM images of unpassivated ZnS:Mn^{2+} nanocrystals. It was found that unpassivated nanocrystals tend to form an aggregation. This is due to a high value of surface to volume ratio. An individual crystal is observed for PSSA-MA passivated sample (Figure 5.3 b). This is indicating that in the presence of PSSA-MA can prevent aggregation among of ZnS crystals. A calculated crystals sizes of unpassivated ZnS:Mn^{2+} nanocrystals were determined to be approximately 3.73 nm in size, and for passivated with PSSA-MA, crystals were 3.38 nm in size. It is shown that in the presence of PSSA-MA, the crystal sizes are smaller than that of no PSSA-MA, which explained that PSSA-MA has an effect on the crystal growth of ZnS:Mn^{2+}. This result leads to the decreasing crystal size. The crystal size that was determined from TEM is corresponding to the result from XRD. The value obtained from TEM is slightly higher than from the XRD. The difference may be due to the crystal size and shape distribution involved and the average value obtained from the calculation.

The lattice fringe (Figure. 5.4 (a) and (b)) is clearly exhibited from an individual nanocrystal. A *d*-spacing among crystal structure was calculated to be 3.051Å. This is in a good agreement with lattice constant of cubic ZnS with a *d* of 3.123 Å for (111) plane [43]. This result was also obtained by Chen et.al.[44]. They found that the (111) lattice spacing of the ZnS:Mn^{2+} particles was estimated to be around 0.31 nm from the HRTEM images. This is consistent with the (111) spacing of bulk ZnS (0.312 nm).

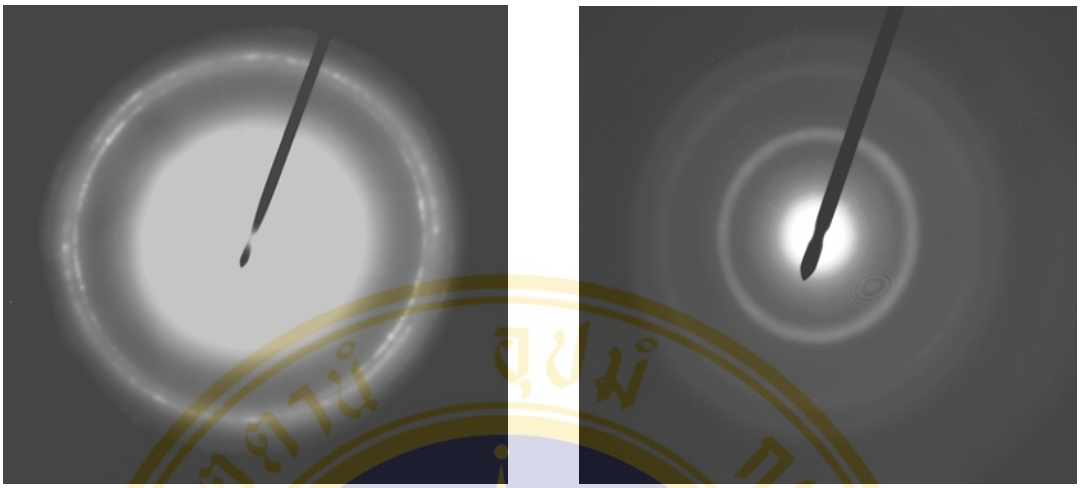

(a) **(b)**

Figure 5.5 Electron diffraction pattern of nanocrystalline ZnS:Mn^2 with (a) and without (b) a passivating of PSSA-MA.

A selected area electron diffraction pattern (ED) of ZnS nanocrystals is shown in figure 5.5 (a). As anticipated, the ED pattern illustrates a set of rings instead of spots. These due to the crystallites have random orientation, which correspond to diffraction from different planes of nanocrystallites. Presence of fine ZnS nanocrystals in polymer matrix is clearly visible in the TEM picture (figure 5.5 (b)), while the corresponding diffraction pattern of the film consists of a central halo with concentric broad rings, the broadness possibly originating from the confinement of the nanocrystallites coated with the PSSA-MA. There are three diffuse rings in the ED pattern, correspond to reflections from the (111), (220) and (311) planes respectively, thus confirming the zinc blende (cubic phase) crystallographic structure of the ZnS nanocrystals. [45]

5.2 UV-Vis absorption spectra

It is well known that the optical band gap of every semiconducting materials increase monotonically with a decrease in the size of the nanocrystallites as followed in equation 3.3. To correlate the size of the nanocrystals with the band gap shift, one compares the calculated variation of band gap as a function of the size with the experimental values from the UV-Vis absorption spectra as the spectra shift systematically to lower wavelengths.

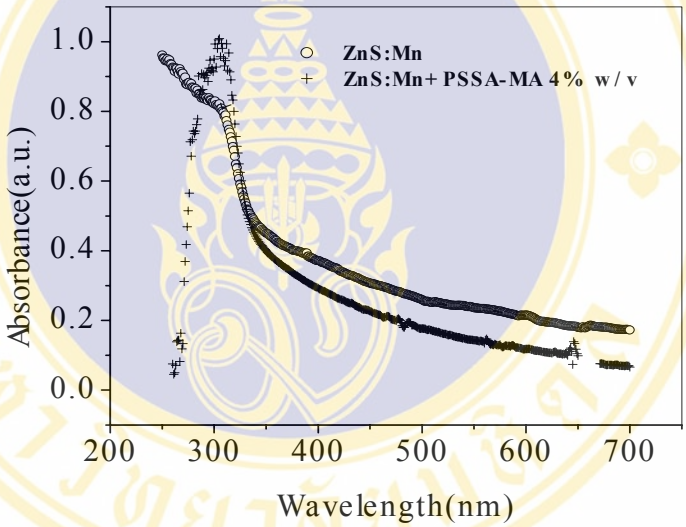

Figure 5.6 UV-Vis absorption of nanocrystalline ZnS:Mn^{2+} without and with a passivating

Figure 5.6 show the UV-Vis absorption spectra of ZnS:Mn^{2+} nanocrystals unpassivated and passivated with PSSA-MA 4% w/v. The aqueous solution and PSSA-MA solution were used as background spectra for measuring absorption of ZnS:Mn^{2+} nanocrystals unpassivated and passivated with PSSA-MA, respectively.

The absorption peaks are difference which is believed to be due to an effect of the light scattering. In the case of no PSSA-MA, the sample solution is cloudy due to the suspension of nanocrystal (The picture of the sample solution is shown in Figure B1 in Appendix B). When the incident light interacts with suspension samples, then

the light scattering occurs in that which leads to have the high absorption intensity. The absorbance reduced until the electron transition was occurred which the spectrum shows shoulder absorption peak. After that the absorption intensity very quickly decreases but it is not equal to zero due to a partial scattering. When the nanocrystals were passivated with PSSA-MA, the sample solution is transparent and leads to the lower light scattering. The absorption intensity at the initial and the last wavelength is nearly equal to zero and the maximum absorption intensity is observed. In addition, the sharpness of absorption peak is believed to be due to a high monodispersity of the sample. A similar phenomenon was observed by Kumbhojkar *et al*.[22]. They have obtained the sharp optical absorption peaks for 1-thioglycerol and thiophenol capped ZnS nanocrystals manifest the high monodispersity of these samples.

From relationship between maximum absorption peak and energy level, the energy gap of the ZnS:Mn^{2+} nanocrystal can be calculated using by equation (5.3), that is

$$\Delta E = h\nu \tag{5.2}$$

or

$$\Delta E = \frac{hc}{\lambda_{max}} \tag{5.3}$$

Where h is Planck's constant.

ν is frequency of light.

c is speed of light.

λ_{max} is maximum absorption wavelength.

From the spectra, the unpassivated ZnS:Mn^{2+} nanocrystals show a shoulder at around 340 nm while the passivated nanocrystals show sharp absorption peak at 304 nm. The spectra shift to the lower wavelength after the nanocrystals were passivated by PSSA-MA. The calculated energy gap is 3.65 eV for unpassivated, 4.08 eV for passivated, and 3.68 eV for bulk ZnS [22], respectively. From the result, it shows that the optical band gap of the passivated nanocrystal is much larger than that of unpassivated and bulk sample. It can be concluded that the crystallize size of

passivated ZnS:Mn^{2+} is smaller than that of unpassivation which corresponding to the result of XRD and TEM.

Figure 5.7 show UV-Vis absorption spectra of passivated nanocrystalline ZnS:$Mn^{2+}$with vary amount of PSSA-MA. The spectra of all samples show sharp absorption peak. As suggested previously, this is certainly due to effect of light scattering and high monodispersity.

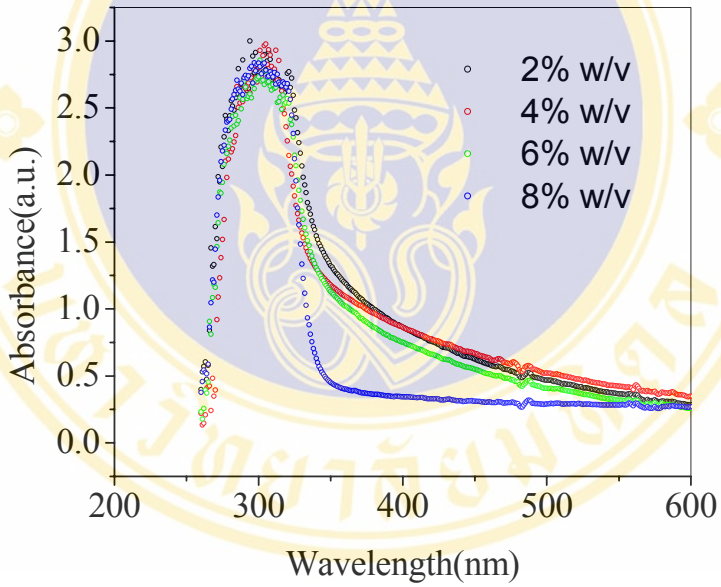

Figure 5.7 UV-Vis absorption of nanocrystalline ZnS:Mn^2 with a passivating of PSSA-MA 2-8% w/v.

5.3 Luminescence and photoluminescence spectra

(a) Before excited by UV-vis (b) After excited by UV-vis

Figure 5.8 Light emission of both passivated nanocrystalline ZnS:Mn^{2+} powder and solution before (a) and after UV-vis excited (b).

Figure 5.8 shows the light emission color both powders and solution of nanocrystalline ZnS:Mn^{2+} with passivated by PSSA-MA before and after excited by UV-Vis light. Figure 5.8 (a), before excitation, the color of nanocrystalline ZnS:Mn^{2+} powders is white and solution is transparent. When the nanocrystals were excited by UV-Vis light, the orange emission of both powders and solution was observed, Figure 5.8 (b).

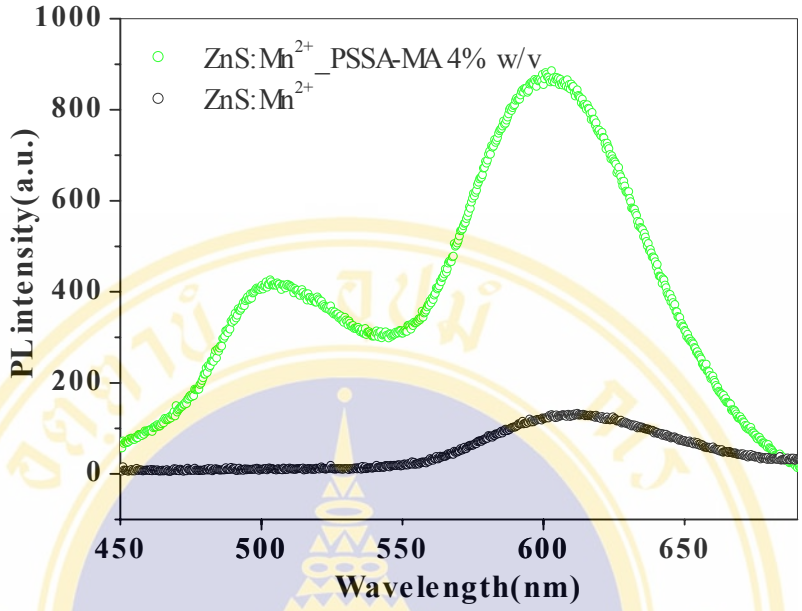

Figure 5.9 Photoluminescence spectra (λ_{exc} = 385 nm) of nanocrystalline ZnS:Mn^{2+} without and with a passivating of PSSA-MA 4% w/v.

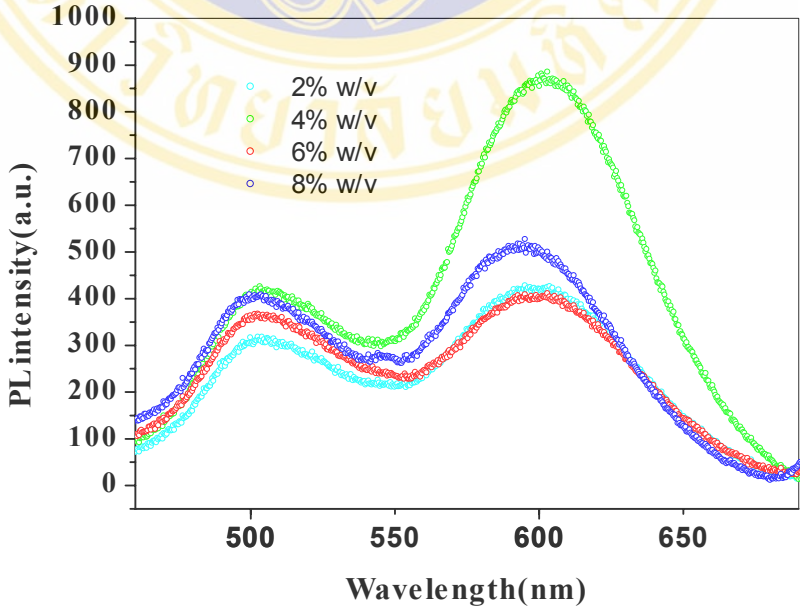

Figure 5.10 Photoluminescence spectra (λ_{exc} = 385 nm) of nanocrystalline ZnS:Mn^{2+} a passivating of PSSA-MA 2-8% w/v.

PL emission spectra (λ_{exc} = 385 nm) (Figure 5.9) of nanocrystalline ZnS:Mn^{2+} powders with and without passivated by PSSA-MA exhibits the orange emission peak at around 600 nm due to a transition between the $^4T_1$ excited state and the $^6A_1$ ground state of the Mn^{2+} ion with in a nanocrystalline ZnS lattice. The broad emission peak around 500 nm, can be assigned to an emission of the PSSA- MA. There is not an emission peak around 500 nm in a PL spectrum of the unpassivated sample. It is also shown that the particles were passivated with PSSA-MA show higher photoluminescence intensity than the samples without passivation. There is no orange emission found from PSSA-MA alone after UV-Vis excitation at 385 nm. An improved in PL is not originated from PSSA-MA but from surface passivated nanocrystals.

This result explained that due to a smallness of ZnS:Mn^{2+} powders without passivation surface, defects such as donors and acceptors are easily formed on the ZnS nanocrystal surface. Since non-radiative recombination occurs through these surface defects, the radiative probability through the Mn^{2+} centers decreases with the increasing surface defects. It is expected that in the presence of PSSA-MA as a surface passivating agent, the surface defects on the nanocrystalline ZnS:Mn^{2+} powders are passivated and eliminated. Hence, an increase of the radiative transition through Mn^{2+} centers is accomplished.

The PL emission spectra of nanocrystalline ZnS:Mn^{2+} with passivated by various amount of PSSA-MA (2-8% w/v) as shown in Figure 5.10. It was found that a maximum PL intensity was observed when using PSSA-MA 4% w/v. This result agrees with that from XRD pattern which shows the smallest crystal size when using PSSA-MA 4% w/v. It is more important to note that PL intensity of nanocrystalline ZnS:Mn^{2+} increases with decreasing crystallite size as followed in equation 3.2.

5.4 X-rays fluorescence (XRF) analysis

The X-ray fluorescence is a tool to analyze elements in the sample. Due to each element characteristic peak, we can detect the component of element in the sample both qualitative and quantitative investigations.

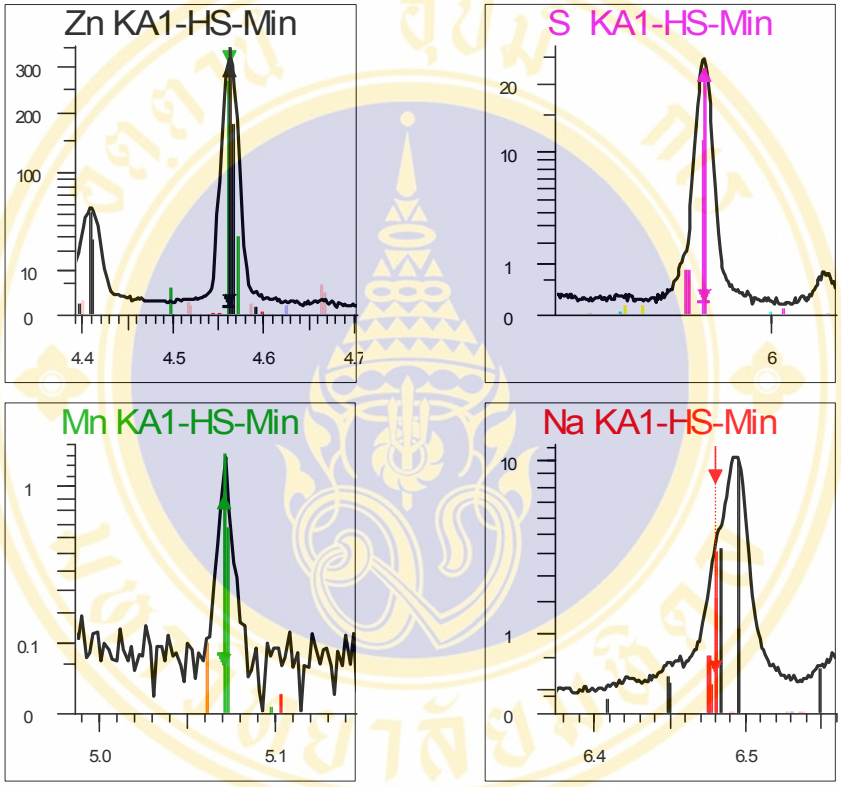

Figure 5.11 XRF spectra of nanocrystalline ZnS:Mn^{2+}passivated with PSSA-MA.

Figure 5.11 shows example of XRF spectra of nanocrystalline ZnS:Mn^{2+} passivated with PSSA-MA 4% w/v. The peak occurs at 4.57, 4.06 and 5.07 eV which correspond to the emission energy of Zn-, S- and Mn-atom, respectively. These results indicate that the presence of Zn-, S- and Mn-elements in the sample. In addition, the peak of Na atom was occurred due to PSSA-MA, sodium salt which was used as passivating agent.

Table 5.2 Mn^{2+} concentration relative to Zn^{2+} determined by XRF (at%) of ZnS:Mn^{2+} passivated without and with PSSA-MA 2-8% w/v

PSSA-MA (%w/v)	Mn/Zn ratio determined by XRF (%at)
0	0.20
2	0.80
4	0.59
6	0.69
8	0.60

The relative ratio amount of Mn^{2+} ions to Zn^{2+} ions in the sample was shown in Table 5.2. It can be seen when the ZnS:Mn^{2+} sample was added with a few amount of PSSA-MA, the ratio amount of Mn^{2+} ions to Zn^{2+} ions increase and gave the maximum ratio when using PSSA-MA 2%w/v. When adding more amount of PSSA-MA, the ratio amount of Mn^{2+} ions to Zn^{2+} ions tends to decrease. This may be due to electrostatic repulsion between the Mn^{2+} ions and Zn^{2+} ions when the nucleation first occurs. When adding polyelectrolyte, it suppressed the repulsion between these two ions. This leads to increasing the amount of Mn^{2+} ions substitution in the Zn^{2+} ions site. When increasing the great amount of PSSA-MA, Mn^{2+} ions substitution in the Zn^{2+} ions decrease. This may be due to the steric hindrance of PSSA-MA which leads to substitution decrease.

5.5 Effect of the Mn^{2+} ion doping concentrations

The effect of the amount of Mn^{2+} on the photoluminescence intensity of passivated and unpassivated with PSSA-MA was investigated.

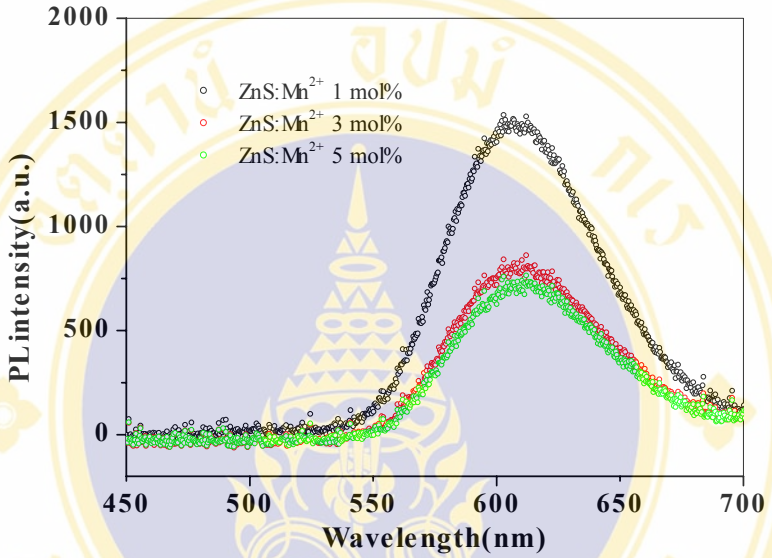

Figure 5.12 Dependence of peak intensity of the photoluminescence (λ_{exc} = 385 nm) on the amount of Mn dopants in unpassivated nanocrystalline ZnS:Mn^{2+}.

The effect of the amount of Mn^{2+} on the photoluminescence intensity of unpassivated sample was shown in Figure 5.12. Photoluminescence measurements show emission maxima at 608 nm from $^4T_1$ - $^6A_1$ transition state in Mn^{2+} ion. Doped samples give varying intensity of emission depending on the concentration of manganese in the sample; the highest intensity measured for ZnS:Mn(1%) samples and the lowest for ZnS: Mn(5%). This result is in agreement with Ihara et al.[20,45]. They explained that, if Mn ions are added in an amount of 1.0% mol, desirably the light emission strength of the entire light emission strength may be increased. Additionally, Yu at.al [6] suggests that considering 1 mol% of Mn doping in the ZnS nano-particles, there are only 4 Mn^{2+} ions on average within such a ZnS nanocrystal.

It suggested that at higher Mn concentration, the isolated Mn ion may stay at the surface or interstitial positions of the crystallites with octahedral symmetry and

these do not favour radiative transitions. Additionally, it was found that the color of sample have changed from white to brown after irradiated by UV-Vis light and then turn to be black-grey color. It shows that the sample will be degradable after irradiated by UV-Vis light. This may be due to surface defect which also lead to non-radiation.

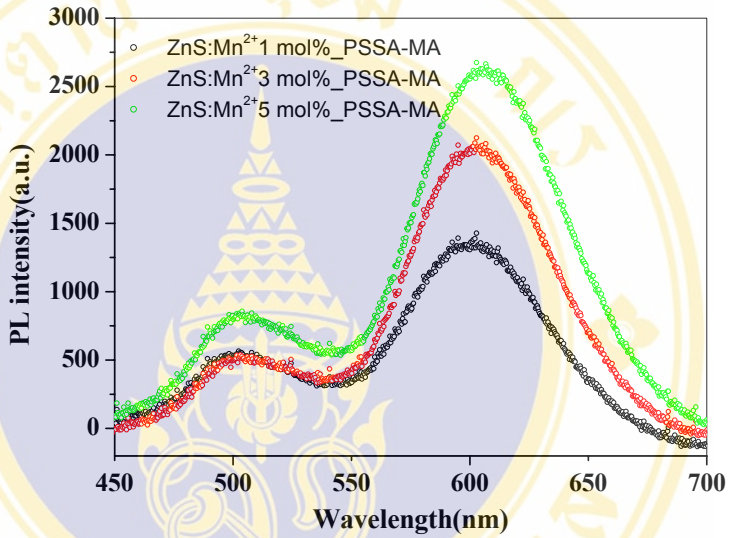

Figure 5.13 Dependence of peak intensity of the photoluminescence (λ_{exc} = 385 nm) on the amount of Mn dopants in nanocrystalline ZnS:Mn^{2+} passivated with PSSA-MA.

Figure 5.13 shows PL emission spectra of ZnS passivated with PSSA-MA and doped with various amount of Mn^{2+}. The spectra show maximum intensity at about 600 nm for transition state in Mn^{2+} ion and 500 nm from emission of PSSA-MA. It implies that when sample was passivated with PSSA-MA, the PL intensity is higher as Mn^{2+} ions are increased. These results differ from previously results. In addition, the color of sample has not changed after irradiated by UV-Vis light. This indicates that the PSSA-MA helps to reduce surface defect of ZnS:Mn^{2+}nanocrystal by decreasing the isolated Mn^{2+} ion that may stay at the surface. This leads to enhancement of the luminescent intensity.

5.6 Effect of PSSA-MA on the Mn^{2+} substitution in the Zn^{2+} site in ZnS

The XRF technique was used for determination the amounts of Zn^{2+} and Mn^{2+} in the samples, and then the Mn/Zn atomic ratios were calculated. The results are shown in Table 5.3 and Figure 5.14. It is found that when ZnS:Mn^{2+} nanocrystals were passivated with PSSA-MA, the concentration of Mn relative to Zn in the nanocrystal sample increased. This result indicates that the amount of Mn^{2+} ion has been replaced the Zn^{2+} ion site increasingly therefore PSSA-MA enhances an efficiency of photoluminescence of Mn^{2+}-doped ZnS nanocrystals.

Table 5.3 Mn^{2+} concentration used in synthesis and determined by XRF (at%) of ZnS:Mn^{2+} passivated without and with PSSA-MA

Mn^{2+} concentration used in synthesis (mol% rel to Zn)	Mn^{2+} concentration measured by XRF (at% rel to Zn)	
	ZnS:Mn^{2+}	ZnS:Mn^{2+}+ PSSA-MA
1	0.11	0.90
3	0.46	2.2
4	0.25	1.7
5	0.27	2.5

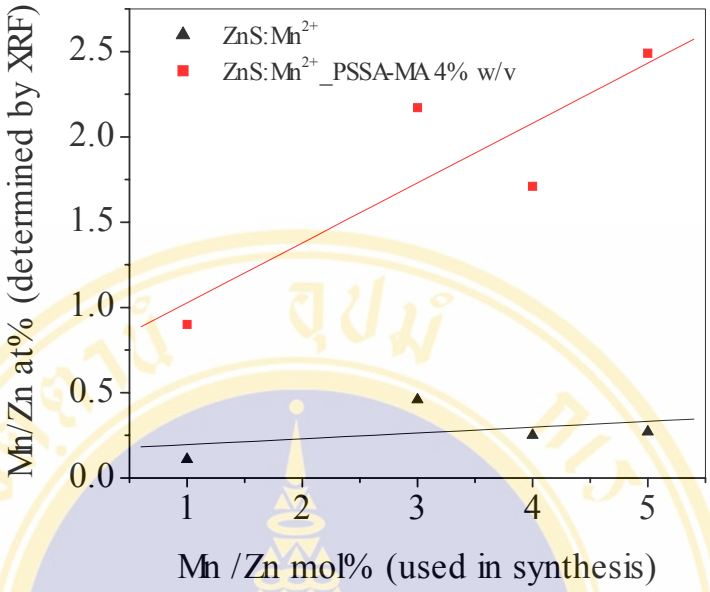

Figure 5.14 Mn $^{2+}$concentrations (at%) are used in ZnS:Mn^{2+} passivated without and with PSSA- MA synthesis are compared with Mn $^{2+}$ concentrations (at%) of ZnS:Mn^{2+} which are analyzed by XRF spectra.

An example of this was investigated by Yang and coworkers [46]. They studied influence of 3-mercaptopropanoic acid (MPA) on the doping of Mn^{2+}. They report that the improvement of the doping efficiency and the reproducibility compared to the common co-precipitation method should be attributed to the introduction of MPA. Since the dissociation constants of ZnS and MnS are $1.1x10^{-24}$ and $2x10^{-13}$ mol L^{-1} respectively, such a large difference makes the co-precipitation of ZnS and MnS very difficult. When Na_2S is added into the solution, the precipitation occurs instantly. The precipitation of ZnS and MnS will be greatly affected by the mixing process which is difficult to control. This will lead to a poor reproducibility of the synthesis. In them case, the MPA is introduced to coordinate with Zn^{2+} before the addition of Na_2S. Due to the coordination, the solubility of ZnS can be increased to $1.1x10^{-6}$ mol L^{-1}, approaching that of MnS. So it can be expected that the co-precipitation of ZnS and MnS is greatly improved.

As suggested previously, it is reasonable to assume our case that the coordination of Zn^{2+} ion with PSSA-MA before Na_2S added; lead to the efficient

doping of Mn^{2+} increase. PSSA_MA polyelectrolyte plays important roles in the enhancement of the luminescent intensity.

5.7 Influence of the surface passivating agent

5.7.1 Passivation of PSSA-MA polyelectrolyte on nanocrystal surface

In order to confirm the presence of surface passivation for the nanocrystalline ZnS:Mn^{2+} prepared by the liquid phase co-precipitation method, FTIR and TGA techniques were used for characterization.

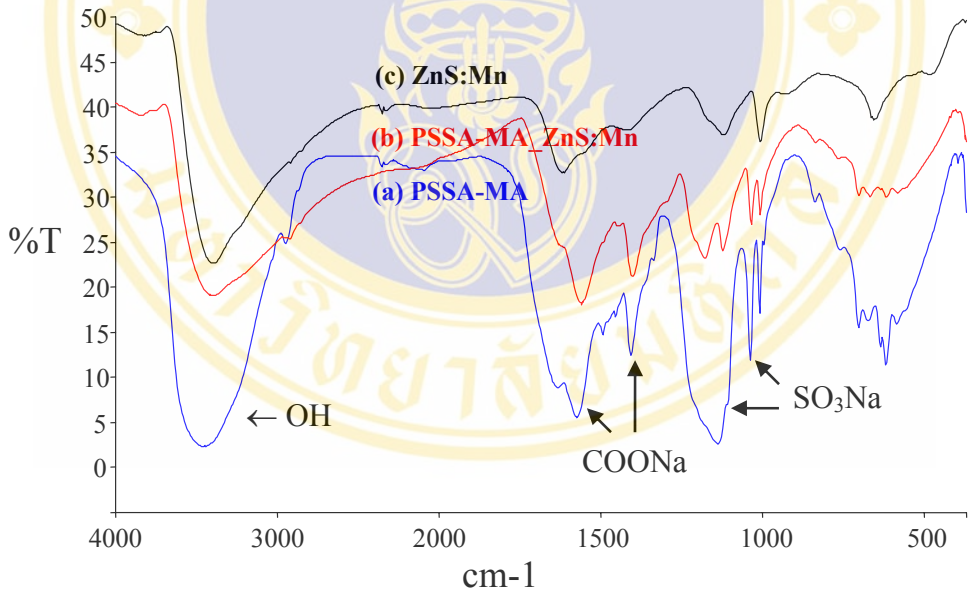

Figure 5.15 Fourier transform infrared (KBr) spectra of (a) PSSA-MA sodium salt, (b) nanocrystalline ZnS:Mn^{2+} passivated with PSSA-MA 4% w/v and (c) nanocrystalline ZnS:Mn^{2+}

Table 5.4 FTIR Band assignments of nanocrystalline ZnS:Mn^{2+}_PSSAMA and PSSA-MA

PSSA-MA	ZnS:Mn^{2+}_PSSAMA	Band assignments
620.08	619.97	C-S stretching of the =C-SO_3^- anion
704.88	704.77	C-H stretching of benzene ring
1010.76	1009.23	In-plane bending of sulfonate group
1039.63	1037.35	Symmetric stretching of sulfonate group(SO_3^-,Na^+)
1140.31	-	Asymmetric stretching of sulfonate group(SO_3^-,Na^+)
-	1180.07	Symmetric bonding of metal ion with asymmetric stretching of SO_3^- group
1409.02	1403.47	Stretching vibration of carboxylate group(COO^- ,Na^+)
1574.93	1560.18	Asymmetric stretching of carboxylate group (COO^- ,Na^+)
1634.21	-	Stretching of phenyl group

Figure 5.15 shows the FTIR spectra of nanocrystal products. The spectrum of poly(4-styrenesulfonic acid-co-maleic acid) sodium salt (Figure 5.15(a)) and unpassivated nanocrystalline ZnS:Mn^{2+} (Figure 5.15(c)) shows the characteristic absorption at 1574 and 1409 cm^{-1} which correspond to stretching vibration of carboxylate groups (COONa). The band at 1574 cm^{-1} is coupled with another band at 1634 cm^{-1} which attributed to the phenyl group. At 1140 and 1039 cm^{-1}, attributed to asymmetric and symmetric absorption band of sulfonate group (SO_3Na), respectively.

The FTIR spectrum of the compound with nanocrystalline ZnS:Mn^{2+} (Figure 5.15 (b)) shows an absorption band at 1560 and 1403 cm^{-1} correspond to stretching vibration of carboxylate groups which coordinated with the zinc ion. The asymmetry band of SO_2 group is observed close to 1180 cm^{-1}, indicating that the sulfonate group is also involved in the coordination. It is possible to suggest a mechanism that involves both sulfonate and carboxylate groups for coordination of the metal ions [36]. In addition, the vibrations in the range 3000-3500 cm^{-1} attributed to O-H stretching of CO_2H and may be due to H_2O that absorbed in the sample.

The absorption band of PSSA-MA on nanocrystalline ZnS:Mn^{2+} particle is thus confirmed, and this leads to the surface passivation.

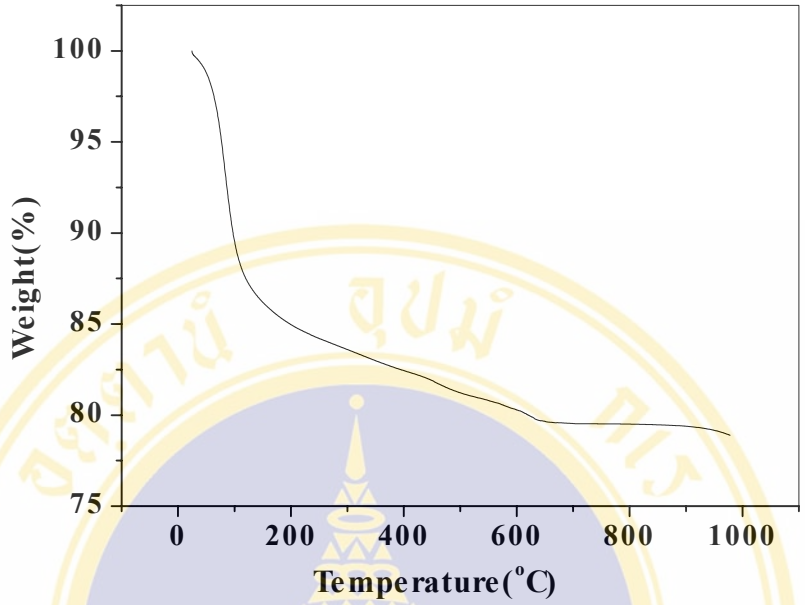

Figure 5.16 TGA curves of ZnS:Mn^{2+} nanocrystalline powder

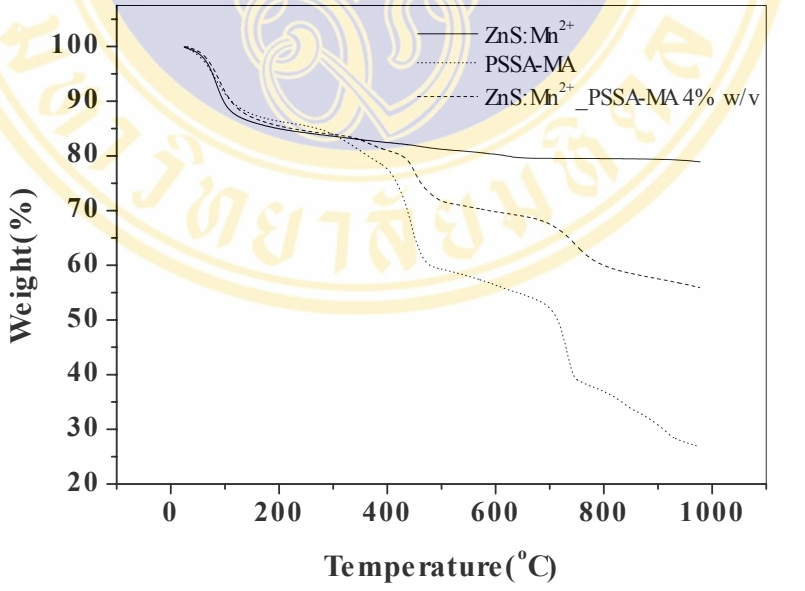

Figure 5.17 TGA curves of ZnS:Mn^{2+} nanocrystalline powder passivated with and without PSSA-MA and PSSA-MA as reference curve.

The TGA curves of ZnS:Mn^{2+} nanocrystal powders are shown in figure 5.16. It presents two weight loss transitions at 97^{o}C and 625^{o}C. The peak at 97 ^{o}C is due to the loss of the absorbed water. The peak at 625^{o}C belongs to a shift in the crystal structure of ZnS. The Figure 5.17 shows the TGA curves of ZnS:Mn^{2+} nanocrystal powders passivated with PSSA-MA, a curve of pure PSSA-MA as reference. The three weight loss transitions were observed when the nanocrystalline ZnS powders were passivated with PSSA-MA. These two peaks were found at 456^{o}C and 748^{o}C have resulted from the decomposition of the PSSA-MA molecule. The results of TGA analyses also confirm that there is PSSA-MA polyelectrolyte in the ZnS:Mn^{2+} nanocrystalline samples. This has also been proved by the IR analyses.

5.7.2 The effect of cleaning by methanol and distilled water

The PSSA-MA passivated on the surface of nanocrystalline ZnS:Mn^{2+} is physical or chemical absorption, which can be proved by FTIR and TGA technique. The samples were prepared with different step in adding PSSA-MA. The prime sample, PSSA-MA was mixed together with zinc and manganese precursor before adding Na_2S. The second one, PSSA-MA was added in the latter step after formed ZnS:Mn^{2+}. Then the nanocrystal products were washed with water and methanol for 3 and 5 times.

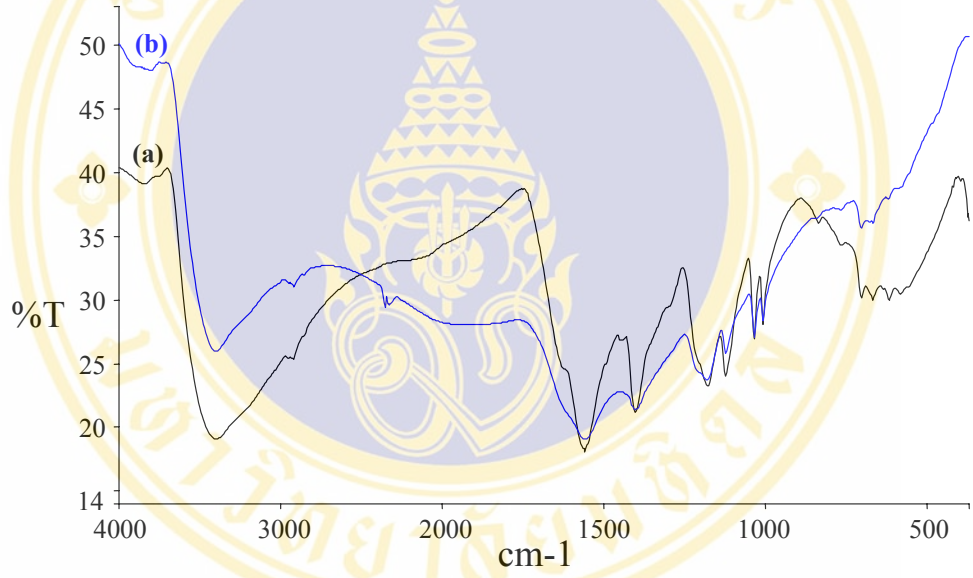

Figure 5.18 Fourier transform infrared (KBr) spectra of nanocrystalline ZnS:Mn^{2+} added with the PSSA-MA 4% w/v at the first step, then washed the nanocrystals 3 (a) and 5(b) times, respectively.

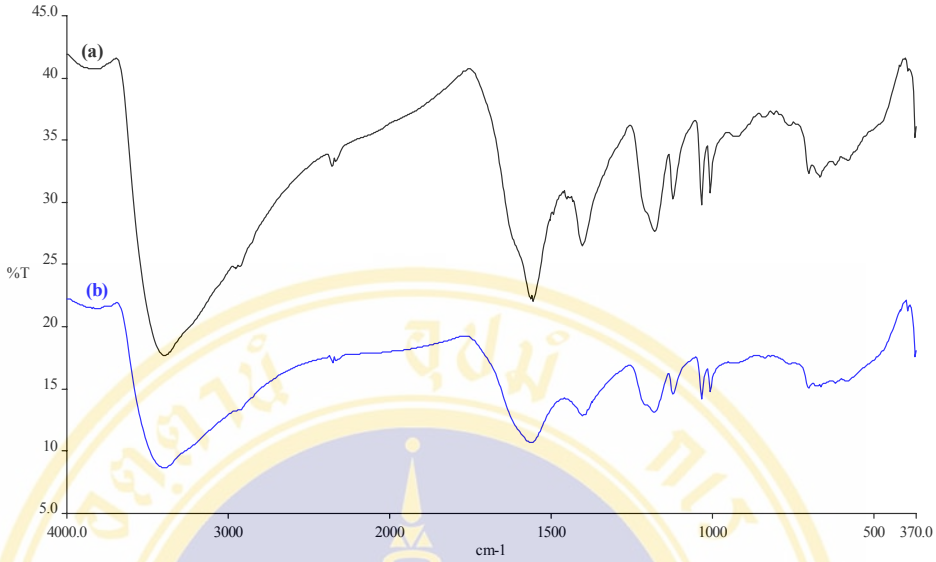

Figure 5.19 Fourier transform infrared (KBr) spectra of nanocrystalline ZnS:Mn^{2+} added with the PSSA-MA 4% w/v at the latter step, then washed the nanocrystals 3 (a) and 5 (b) times, respectively.

Figure 5.18 show the FTIR spectra of nanocrystalline ZnS:Mn^{2+} added with the PSSA-MA (4% w/v) in the first step and washed with good solvent for 3 times as shown in figure 5.18 (a). The sample washed with solvent raise to 2 times. The FTIR spectra (figure 5.18 (b)) still presence absorption band of two functional groups which coordinating with metal ion. The FTIR spectra of the nanocrystalline ZnS:Mn^{2+} added with PSSA-MA in the latter step as shown in figure 5.19. The obtained result is similar to the previous case. This may indicate that the PSSA-MA which is adsorbed on the ZnS:Mn^{2+} nanocrystal surface by bond formation, independent on adding steps of surface passivating agent and PSSA-MA wash-up is not effect to break bond between functional group of polymer and nanocrystal surface.

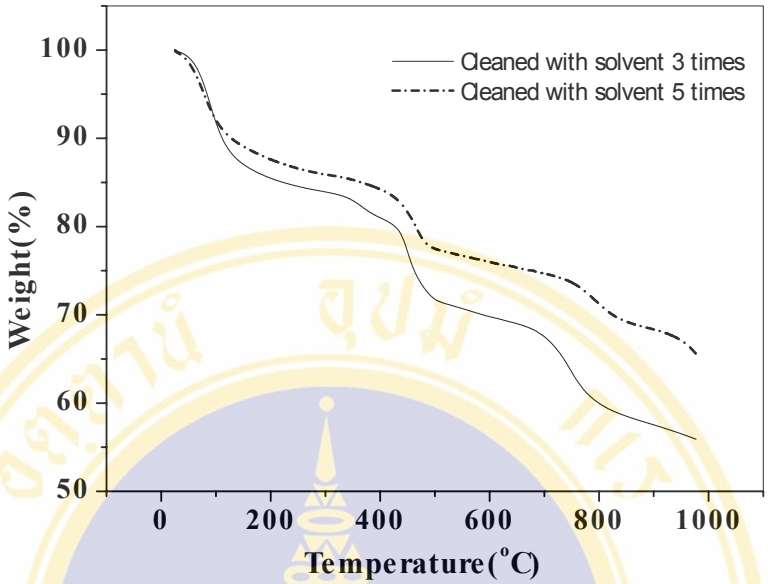

Figure 5.20 TGA curve of nanocrystalline ZnS:Mn^{2+} added with the PSSA-MA 4% w/v at the first step, then washed the nanocrystals 3 (solid line) and 5 times (dash line), respectively.

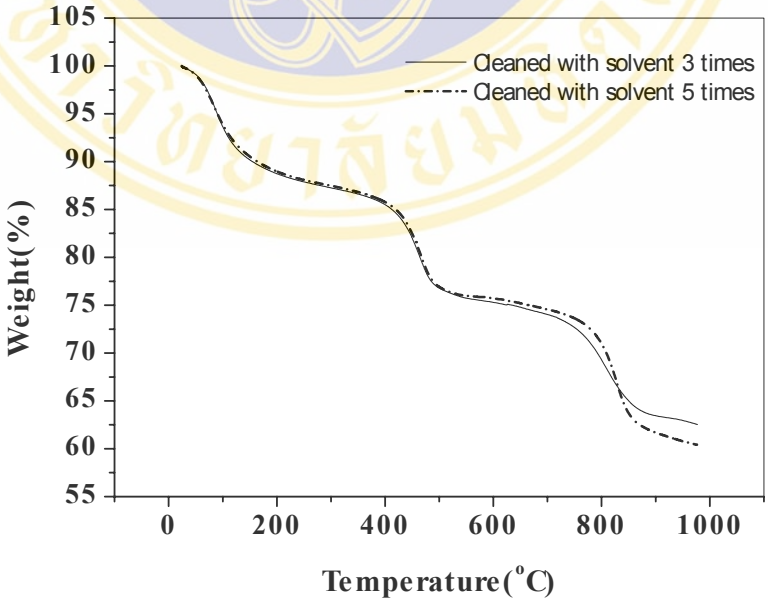

Figure 5.21 TGA curve of nanocrystalline ZnS:Mn^{2+} added with the PSSA-MA 4% w/v at the latter step, then washed the nanocrystals 3 (solid line) and 5 times (dash line), respectively.

Table 5.5 Percent weight loss of PSSA-MA

Sample	Weight loss (%)	
	Washed with solvent 3 times	Washed with solvent 5 times
Added PSSA-MA in the first step	26.4	14.9
Added PSSA-MA in the latter step	24.6	27.0

The TGA curve of nanocrystalline ZnS:Mn^{2+} added with the PSSA-MA at the first step and washed with methanol solvent (considered as a good solvent) 3 and 5 times, respectively as shown in figure 5.20. The percent weight loss of PSSA-MA after washed sample 3 times is 26.4% (Table 5.5). When the nanocrystals were increasingly washed, the percent of PSSA-MA decrease to be 14.9%**.** The weight loss has been decreased may be due to after washed sample with solvent 5 times, non-interacted PSSA-MA has been removed. A comparison with the sample added with PSSA-MA in the latter step shows the total weight loss of 24.6% for washed sample 3 times and 27.0% for washed sample 5 times which had been evaluated from figure 5.21. This shows that, PSSA-MA interact with surface of nanocrystalline ZnS:Mn^{2+} by different bond formation or it is possible that there may be a different incorporation of the polymer into ZnS:Mn^{2+} crystal. However, the nanocrystalline sample added with the PSSA-MA at the first step shows higher photoluminescence.

CHAPTER VI

CONCLUSION

A synthesis of Mn^{2+}-doped ZnS ($ZnS:Mn^{2+}$) nanocrystal material was synthesized by a liquid phase co-precipitation method at room temperature in the presence of poly(4-styrenesulfonic acid-co-maleic acid) (PSSA-MA), sodium salt as a surface-passivating agent. In this study, the crystal structure, crystal size and the optical properties of passivated nanocrystal material are reported and compared to those of unpassivated. Additionally, the relationships between the crystal size and optical properties of sample are also discussed. The sample composition was investigated by XRF. It was found that the Zn-, S- and Mn-atoms are present in the sample. The 1 mol% doped concentration of Mn^{2+} in ZnS nanocrystal powder was selected as a model system in the study othe effect of passivating agent on the luminescent process. The structure of the synthesized $ZnS:Mn^{2+}$ nanocrystal metarials that determined from diffraction angle of XRD and TEM are cubic structure (zinc blende). The XRD peaks are broaden, showing that the small crystals are formed in the sample. The calculated crystal size from the width of XRD peaks broadening via the Debye-Scherrer formula and the TEM imaging showing the average crystal size of passivated samples is 2-3 nm which is smaller than that of unpassivation sample. This indicates that the passivation of PSSA-MA can inhibit the crystal growth of $ZnS:Mn^{2+}$ materials. This result is in agreement with the size observed from TEM. The variation of band gap was calculated as a function of the size with the experimental values from the UV-Vis absorption spectra. The $ZnS:Mn^{2+}$ passivated with PSSA-MA 4% w/v is selected to study this correlation, comparison with unpassivating and bulk sample. The unpassivated sample having 2.70 nm in size showing the optical band gap is about 3.65 eV while passivated sample having 2.24 nm in size showing the optical band gap is about 4.08 eV. Additionally, the optical band gap of bulk material is 3.67 eV. These results indicate that the optical band gap increased with decreasing crystallite size.

The photoluminescence (PL) of samples shows an orange emission peak at 600 nm which characterize for the $^4T_1 \rightarrow {}^6A_1$ transition of Mn^{2+} ion in a crystalline ZnS-matrix. PL enhancement has been observed after passivated with PSSA-MA. This is achieved by eliminating the surface defects and the depressed radiationless transitions. The highest PL intensity was obtained when using PSSA-MA 4% w/v.

The results from FTIR and TGA confirm the presence of PSSA-MA in the nanocrystal samples. The FTIR spectra show absorption peak shift of sulfonate and carboxylate group after sample passivated with PSSA-MA. The peak shift indicates that there is coordination of both functional groups with nanocrystal sample.

An effect of washing on in the presence of PSSA-MA was found that there are still some absorption bands of sulfonate and carboxylate group. The coordinating of PSSA-MA with metal ion is present. This is possible that there may be a bond formation or an incorporation of the polymer into ZnS:Mn^{2+} crystal.

The above conclusions indicate that Mn^{2+}-doped ZnS metarial having nanocrystal size and enhanced photoluminescence have been synthesized by a liquid phase co-precipitation method at room temperature in the presence of poly(4-styrene sulfonic acid-co-maleic acid) (PSSA-MA) as a surface-passivating agent.

REFERENCES

1. Lu HY and Chu SY. The mechanism and characteristics of ZnS-based phosphor powders. J Cryst Growth. 2004; 265: 476-481.
2. Falcony C, Garcia M, and Ortiz A. Luminescent properties of ZnS:Mn films deposited by spray pyrolysis. J Appl Phys. 1992; 72: 1525-1527.
3. Yang H, Wang Z, Song L, Zhao M, Chen Y, Dou K, Yu J and Wang L. Study of optical properties of manganee doped ZnS nanocrystals. Mater Chem Phys. 1997; 47: 249-251.
4. Pingbo X, Weiping Z, Min Y, Houtong C, Weiwei Z, Liren L and Shangda X. Photoluminescence properties of surface-modified nanocrystalline ZnS:Mn. J Collo Inter Sci. 2000; 229: 534-539.
5. Yang H, Zhao J, Song L, Shen L, Wang Z, Wang L and Zhang D. Photoluminescent properties of ZnS:Mn nanocrystals prepared inhomogeneous system. Mater Lett. 2003; 57: 2287-2291.
6. Karar N, Singh F and Mehta BR. Structure and photoluminescence stydies on ZnS:Mn nanoparticles. J Appl Phys. 2004; 93(2): 656-660.
7. Yu IL, Isobe T and Senna M.Optical properties an characteristic of ZnS nanoparticles with homogenous Mn distribution. J Phys Chem Solids. 1996; 57(4): 373-379.
8. Yang H and Holloway PH. Photoluminescent and electroluminescent propertiesof Mn-doped ZnS nanocrystals. J Appl Phys. 2003; 93 (1): 586-592.
9. Tang W and Cameron DC. Electroluminescent zinc sulphide devices produced by sol-gel processing. Thin Solid Films. 1996; 280: 221-226.

10. Bhagava RN, Gallagher D, Dong X and Nurmikko A. Optical properties of manganese-doped nanocrystals of ZnS. Phys Rev Lett. 1994; 72: 416-419.

11. Bhargava RN. Doped nanocrystalline materials — Physics and applications. J Lumin. 1996; 70: 85.

12. Bol AA, Meijerink A, . Long-lived Mn^{2+} emission in nanocrystalline ZnS:Mn^{2+} Phys Rev B. 1998; 58: 15997-16000.

13. Horii Y, Kitagawa M, Taneoka H, Kusano H, Murakami T, Hino Y and Kobayashi H. Electrolmnescence properties of PVCz electroluminescent devices doped with nano-crystalline particles. Mater Sci Engin. 2001; 85: 92-95

14. Horng RH, Wuu DS and Yu JW. An electroluminescent device using multi-barrier Y_2O_3 layers incorporated into ZnS:Mn phosphor layer . Mater Chem Phys. 1997; 51: 11-14.

15. Bruchez MJ, Moronne M, Gin P, Weiss S and Alivisatos AP. Semiconductor nanocrystals as fluorescent biological levels. Scince. 1998; 281: 2013-2015

16. Chan WCW and Nie S. Quantum dot bioconjugates for ultrasensitive nonisotopic detection. Scince. 1998; 281: 2016-2018.

17. Kortan AR, Hull R, Opila RL, Bawendi MG, Steigerwald ML, Carroll PJ and Brus LE. J. Am. Chem. Soc. 1990; 112: 1327.

18. Stucky GD and MacDougall JE, science, 1990; 247: 669.

19. Lu SW, Lee BI, Wang ZL, Tong W, Wagner BK, Park W and Summers CJ. Synthesis and photoluminescence enhancement of Mn^{2+}-doped ZnS nanocrystals. J Lumin. 2001; 92: 73-78.

20. Ihara M, Takahiro I, Kusunoki T, Ohno K, Senna M, Isobe T and Konishi M. Method for producing light emitting substrace. US 6,447,698 B1. 2002.

21. Dautzenberg H, Jaeger W, Kotz J, Philipp B, Seidel CH and Stscherbina. Polyelectrolytes formation, characterization and application. Hanser New York. 1994

22. Kumbhojkar N, Nikesh VV, Kshirsagar A and Mahamuni S. Photophysical properties of ZnS nanoclusters. J Appl Phys. 2000; 88(11): 6260- 6264.

23. Konisi M, Isobe T and Senna M. Enhancement of photoluminescence of ZnS:Mn nanocrystals by hybridizing wth polymerized acrylic acid. J Lumin. 2001 ; 93: 1-8

24. Yang H, Han S, Cui Y, and Liang Y. Enhancement of photoluminescent intensity of ZnS:Mn nanocrystals coated with the polymers. Mater Lett. 2004; 58: 2087-2090.

25. Lee BI and Lu SW. Synthesis of nanoparticles via surface modification for electronic applications. J Ceram. Proc. Res. 2000; 1: 20-26.

26. Bol AA, Meijerink. Luminscence quantum efficiency of nanocrystallineZnS:Mn^{2+}. 1. surface passivation and Mn^{2+} concentration. J. Phys. Chem. B. 2001; 105: 10197-10202.

27. Azaroff LV and Brophy JJ. Electronic process in materials. International student addition. New York. McGraw-Hill, Inc. 1963.

28. http://chemed.chem.purdue.edu/genchem/topicreview/bp/ch13/unitcell.html

29. Gan LM, Liu B, Chew CH, Xu SJ, Chua SJ, Loy GL and Xu GQ, Enhanced Photoluminescence and Characterization of Mn-Doped ZnS Nanocrystallites Synthesized in Microemulsion. Langmuir. 1997**;** 13: 6427-6431.

30. Manzoora K, Vaderaa SR, Kumara N and Kutty TRN. Energy transfer from organic surface adsorbate-polyvinyl pyrrolidone molecules to luminescent centers in ZnS nanocrystals. Solid State Communications 2004; 129: 469–473

31. Moriarty P. Nanostructured materials. Rep. Prog. Phys. 2001; 64: 297–381.

32. Brus LE**.** J. Chem. Phys. 1984; 80: 4403.

33. Wang Y, Herron N, Moller K and Bein T. Solid State Commun. 1991; 77: 33.

34. Jin C, Yu J, Sun L, Dou K, Hou S, Zhao J, Chen Y, Huang S. Luminescence of Mn^{2+} doped ZnS nanocrystallites. J. Lumin 1996; 66&67: 315-318.

35. Chen S and Liu W. Preparation and Characterization of Surface-Coated ZnS Nanoparticles. Langmuir. 1999; 15: 8100-8104.

36. Rivas BL, Seguel GV, Geckeler KE. Synthesis, Characterization, and Properties of Polychelates of Poly(Styene Sulfonic Acid-*co*-Maleic Acid) With Co(II), Cu(II), Ni(II), and Zn(II). J. App. Polym. Sci. 2002; 85: 2546–2551.

37. Kane RS and Cohen RE. Semiconductor Nanocluster Growth within Polymer Films. Langmuir. 1999; 15: 39-43)

38. Velev OD and Nagayama K. Assembly of Latex Particles by Using Emulsion Droplets. 3. Reverse (Water in Oil) System. Langmuir 1997; *13:* 1856-1859.

39. Co¨lfen H and Antonietti M. Crystal Design of Calcium Carbonate Microparticles Using Double Hydrophilic Block Copolymers. Langmui. 1998; *14:* 582-589.

40. Precipitation of Inorganic Salts inside Hollow Micrometer-Sized Polyelectrolyte Shells. Journal of Colloid and Interface Science. 2002; 247: 251–254.

41. Cullity BD, Stock SR. Elements of X-ray Diffraction Second edition: Addison-Wesley Publishing Company, Inc.1978 100.

42. Feynman RP. IEEE J. There's plenty of room at the bootom. Microelectromechanical Systems. 1992; 1: 60-67.

43. Flynn CE, Mao C, Hayhurst A, Williams JL. Georgiou G, Iversona B and Belcher AM. Synthesis and organization of nanoscale II–VI semiconductor materials using evolved peptide specificity and viral capsid assembly. J. Mater. Chem. 2003; 13: 2414–2421.

44. Chen W, Joly AG, Malm JO, Bovin JO and Wang S. Full-Color Emission and Temperature Dependence of the Luminescence in Poly-*P*-phenylene ethynylene-ZnS/Mn^{2+} Composite Particles. J. Phys. Chem. B. 2003; 107: 6544-6551.

45. Bhattachajee B, Ganguli D, Iakoubouvskii K, Stesmans A and Chaudhuri S. Synthesis and characterization of sol-gel derived ZnS:Mn^{2+} nanocrystallites embedded in a silica matrix. Bull. Mater. Sci. 2002; 25(3): 175-180.

46. Zhuang J, Zhang X, Wang G, Li D, Yang W and Lia T. Synthesis of water-soluble ZnS : Mn^{2+} nanocrystals by using mercaptopropionic acid as stabilizer. J. Mater. Chem., 2003; 13: 1853–1857.

APPENDIX

APPENDIX A

Instruments

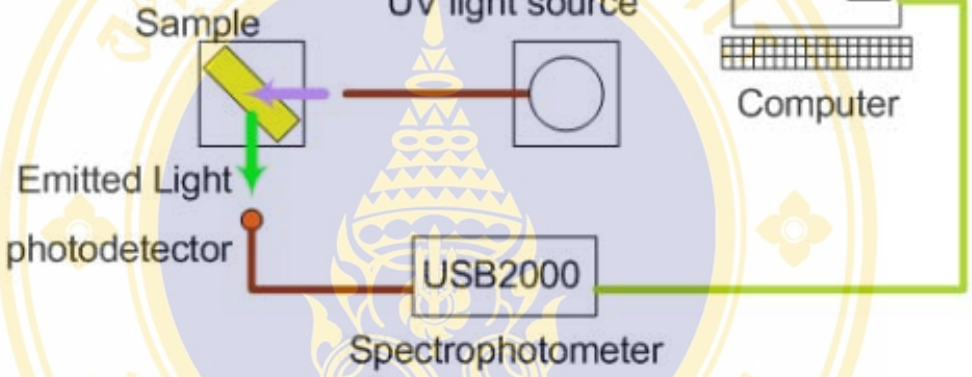

Figure A1 Layout of the experiment set-up for the photoluminescence emission spectra measurement and analysis.

APPENDIX B

Sample solution

(a) (b) (c) (d)

FigureB**1** The solution of ZnS (a), ZnS:Mn^{2+}(b), ZnS:Mn^{2+} passivated with PVP (c) and ZnS:Mn^{2+} passivated with PSSA-MA(d), respectively

APPENDIX C

TGA profiles

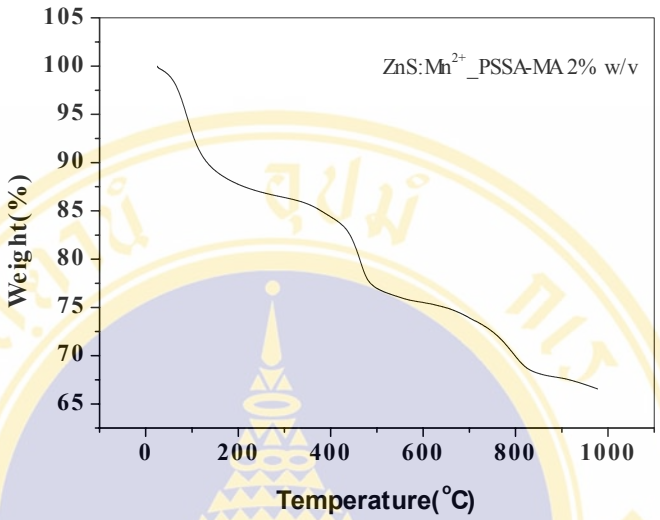

Figure C1. TGA curves of ZnS:Mn^{2+} nanocrystalline powder passivated with PSSA-MA 2% w/v.

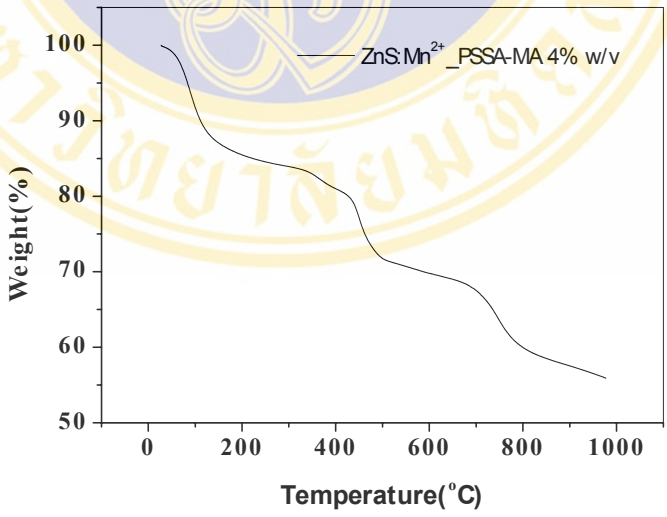

Figure C2. TGA curves of ZnS:Mn^{2+} nanocrystalline powder passivated with PSSA-MA 4% w/v.

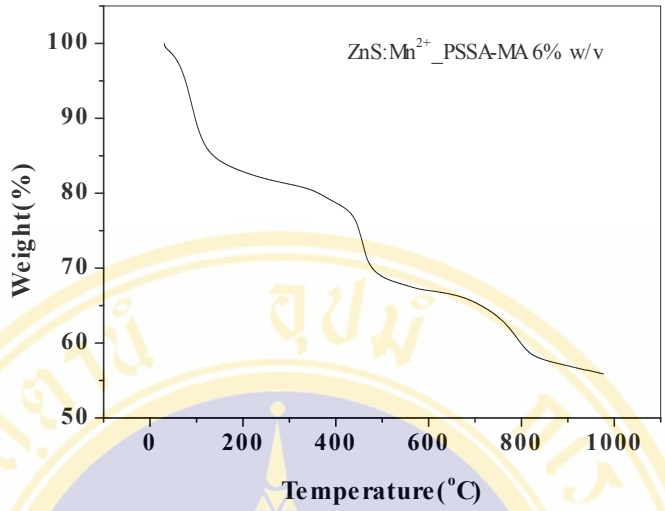

Figure C3. TGA curves of ZnS:Mn^{2+} nanocrystalline powder passivated with PSSA-MA 6% w/v.

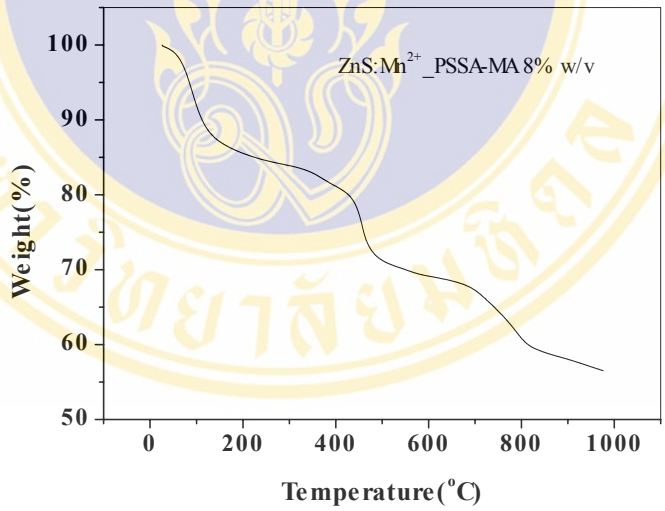

Figure C4. TGA curves of ZnS:Mn^{2+} nanocrystalline powder passivated with PSSA-MA 8% w/v.

APPENDIX D

FTIR spectra

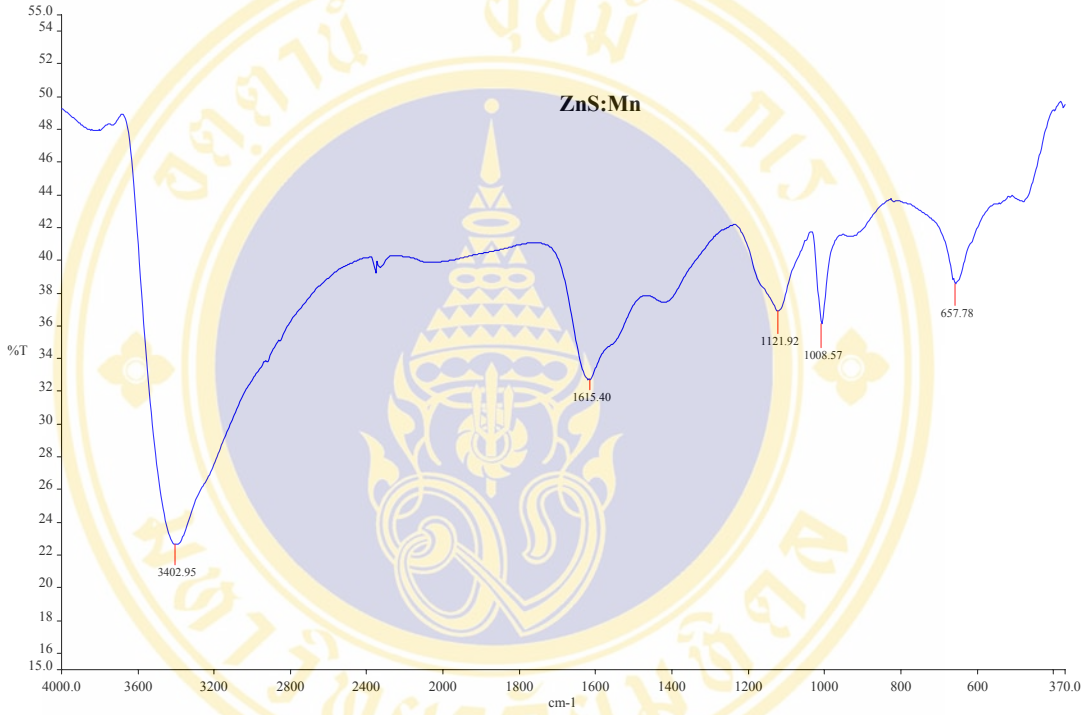

Figure D1 FTIR spectra of nanocrystalline ZnS:Mn^{2+} material

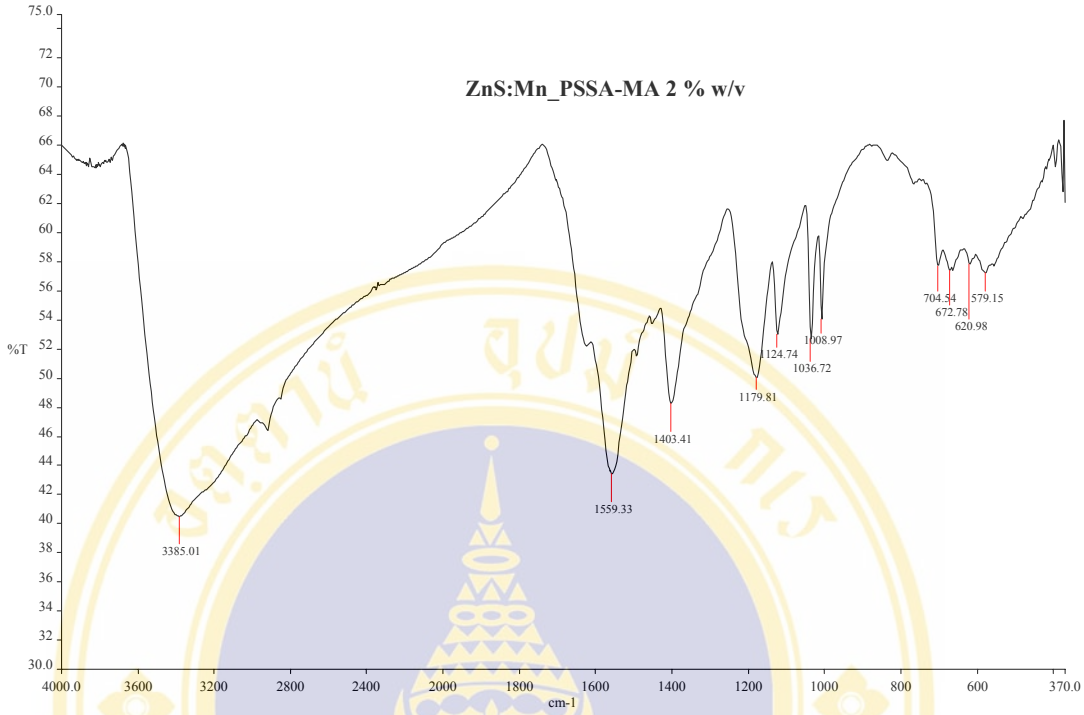

Figure D2 FTIR spectra of nanocrystalline ZnS:Mn^{2+} passivated with PSSA-MA 2%w/v

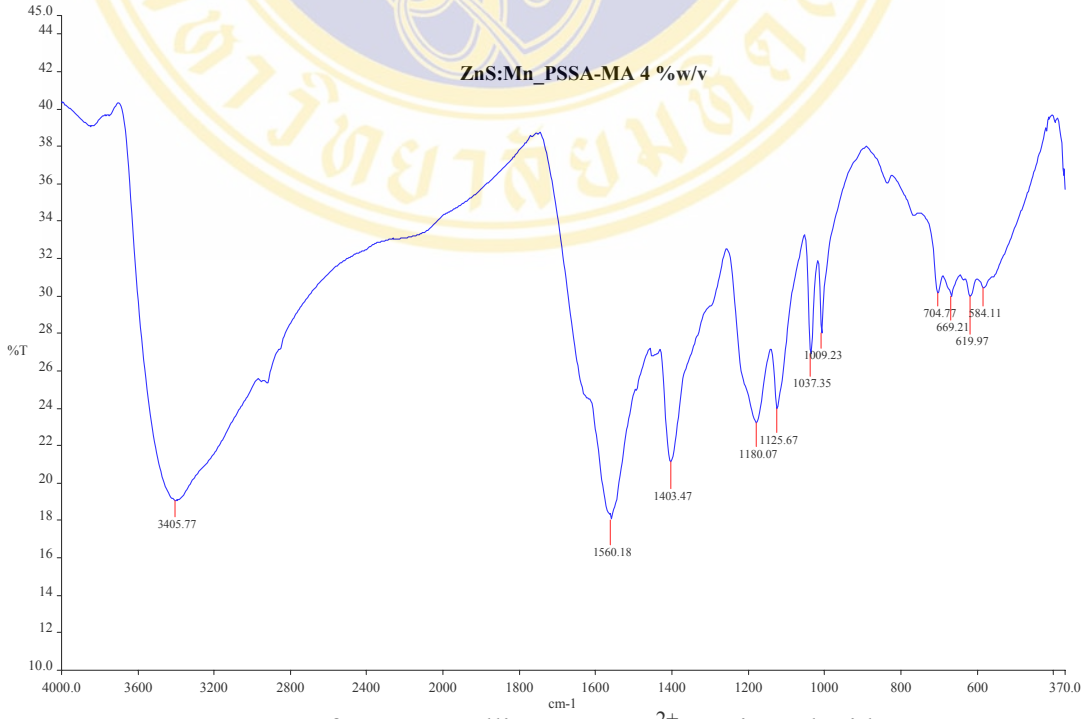

Figure D3 FTIR spectra of nanocrystalline ZnS:Mn^{2+} passivated with PSSA-MA 4% w/v

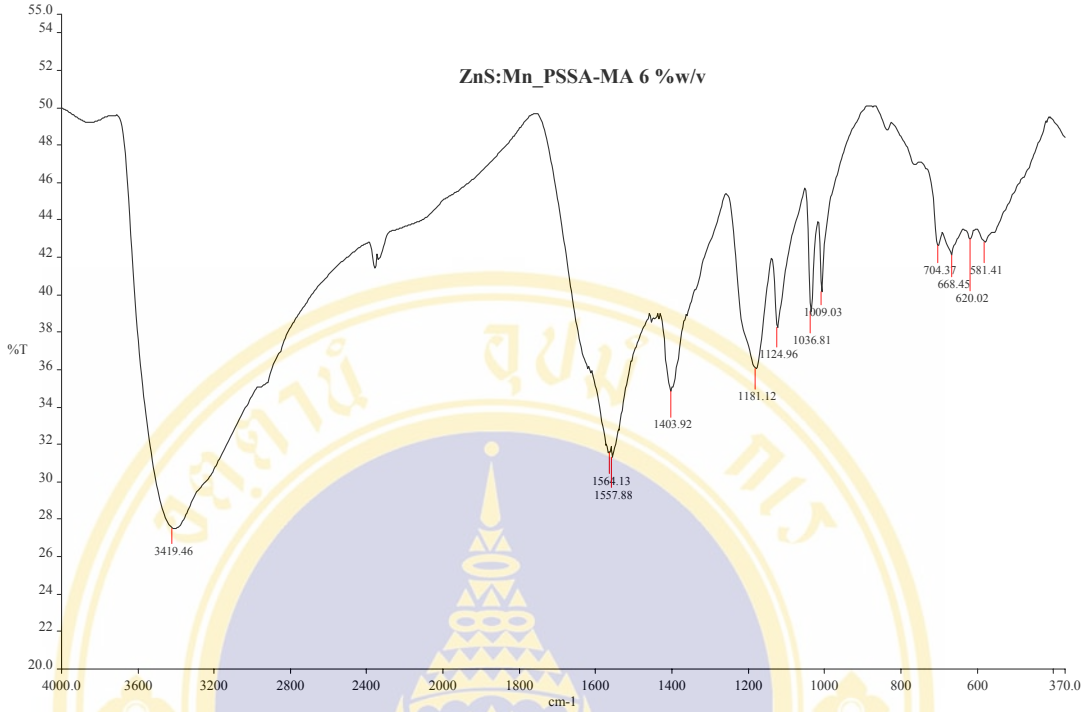

Figure D4 FTIR spectra of nanocrystalline ZnS:Mn^{2+} passivated with PSSA-MA 6% w/v

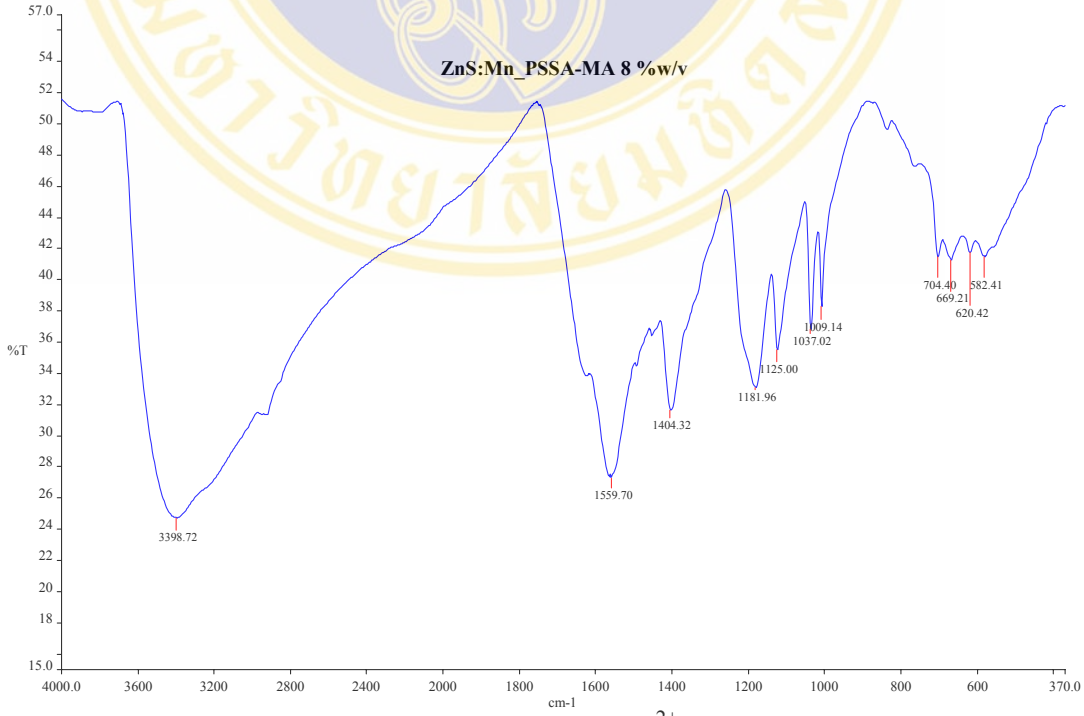

Figure D5 FTIR spectra of nanocrystalline ZnS:Mn^{2+} passivated with PSSA-MA 8% w/v

BIOGRAPHY

NAME	Miss. On-uma Nimittrakoolchai
DATE OF BIRTH	16 August 1979
PLACE OF BIRTH	Nakornpatom, Thailand
INSTITUTIONS ATTENDED	Mahidol University, 1998-2001: Bachelor of Science (Chemistry) Mahidol University, 2002-2004: Master of Science (Polymer Science and Technology)
RESEARCH GRANT	Teaching Assistant Scholarship, Faculty of Science, Mahidol University
HOME ADDRESS	72/364 Park Gallery Suan Thon Village Rattanathibeth Road A. Muang Nonthaburi Thailand
E-MAIL	onn_nimit@yahoo.com